Mon. Not. R. Astron. Soc. **372,** 933–948 (2006) doi:10.1111/j.1365-2966.2006.10918.x

Natural downsizing in hierarchical galaxy formation

Eyal Neistein,[1]★ Frank C. van den Bosch[2]★ and Avishai Dekel[1]★

[1]*Racah Institute of Physics, The Hebrew University, Jerusalem, Israel*
[2]*Max-Planck-Institute for Astronomy, Königstuhl 17, D-69117 Heidelberg, Germany*

Accepted 2006 August 3. Received 2006 July 3; in original form 2006 May 1

ABSTRACT

Stellar-population analyses of today's galaxies show 'downsizing', where the stars in more massive galaxies tend to have formed earlier and over a shorter time-span. We show that this phenomenon is not necessarily 'antihierarchical' but rather has its natural roots in the bottom-up clustering process of dark-matter haloes. While the main progenitor does indeed show an opposite effect, the integrated mass in all the progenitors down to a given minimum mass shows a robust downsizing that is qualitatively similar to what has been observed. These results are derived analytically from the standard extended Press–Schechter (EPS) theory, and are confirmed by merger trees based on EPS or drawn from *N*-body simulations. The downsizing is valid for any minimum mass, as long as it is the same for all haloes at any given time, but the effect is weaker for smaller minimum mass. If efficient star formation is triggered by atomic cooling, then a minimum halo mass arises naturally from the minimum virial temperature for cooling, $T \simeq 10^4$ K, though for such a small minimum mass the effect is weaker than observed. Baryonic feedback effects, which are expected to stretch the duration of star formation in small galaxies and shut it down in massive haloes at late epochs, are likely to play a subsequent role in shaping up the final downsizing behaviour. Other appearances of downsizing, such as the decline with time of the typical mass of star-forming galaxies, may not be attributed to the gravitational clustering process but rather arise from the gas processes.

Key words: galaxies: elliptical and lenticular, cD – galaxies: haloes – cosmology: theory – dark matter.

1 INTRODUCTION

A key issue in the study of galaxy formation is the anticorrelation between the stellar mass of a galaxy and the formation epoch of the stars in it, which is referred to in general terms as 'downsizing'. In its most pronounced form, this is simply the fact that elliptical galaxies consist of old stellar populations and tend to be more massive, while disc galaxies have younger stars and are typically less massive. However, a similar correlation between stellar mass and age is detected within each of the two major classes of galaxies, whether they are classified morphologically as ellipticals versus spirals or by colour as 'red-sequence' versus 'blue-sequence' galaxies. These trends are quite robust, for example, they are insensitive to how luminosity is translated to stellar mass and colour to stellar age.

A downsizing effect can actually appear in different forms which refer to different phenomena, involving different types of galaxies and different epochs in their histories. One form, which is the main focus of the current paper, is the fact that the star formation histories inferred from present-day galaxies using synthetic stellar evolution models correlate with galactic stellar mass. The stars in more massive galaxies tend to form at an earlier epoch and over a shorter time-span. This phenomenon is termed 'archaeological downsizing' (ADS; following Thomas et al. 2005). Using observed line indices and abundance ratios, ADS has been detected in elliptical galaxies (Nelan et al. 2005; Thomas et al. 2005), and in a large sample of galaxies from the Sloan Digital Sky Survey (Heavens et al. 2004; Jimenez et al. 2005).

The other face of downsizing is the fact that the sites of active star formation shift from high-mass galaxies at early times to lower mass systems at lower redshift. We term this phenomenon 'downsizing in time' (DST). It has first been detected by Cowie et al. (1996), who found that the maximum rest-frame *K*-band luminosity of galaxies undergoing rapid star formation has been declining smoothly with time in the redshift range $z = 0.2$–1.7. This DST phenomenon has been confirmed by numerous subsequent studies (Guzman et al. 1997; Brinchmann & Ellis 2000; Kodama et al. 2004; Bell et al. 2005; Bundy et al. 2005; Juneau et al. 2005).

It is important to realize that these two forms of downsizing can be very different, and possibly even orthogonal to each other. The archaeological analysis of local galaxies highlights the formation epoch of the majority of their stars, which at least in the case of ellipticals occurs at high redshifts, $z \sim 2$–5. In contrast, DST refers

★E-mail: eyal_n@phys.huji.ac.il (EN); vdbosch@mpia-hd.mpg.de (FCvdB); dekel@phys.huji.ac.il (AD)

to the specific star formation rate (SSFR) at relatively low redshifts, $z \lesssim 1$, and therefore focuses on later phases of star formation, which may involve only a small fraction of the stars in the galaxy. Unless the stellar-mass ranking of present-day galaxies is the same as that of their progenitors at higher redshifts, these two forms of downsizing do not necessarily reflect the same phenomenon. Since hierarchical clustering in general does not preserve this mass ranking, the two forms of downsizing should be treated as two different phenomena. Indeed, as we will demonstrate below, the understanding of one does not imply an understanding of the other.

In the standard Λ cold dark matter (ΛCDM) cosmological scenario, dark-matter (DM) haloes are built hierarchically bottom up. This is obvious for the evolution of individual haloes, as they are constructed by the gradual gravitational assembly of smaller progenitor haloes that have collapsed and virialized earlier on. The bottom-up clustering can also be inferred statistically from the power spectrum of initial density fluctuations, which indicates that the mass distribution of collapsing systems is shifting in time from small to large masses. These hierarchical aspects of the clustering process have led to the misleading notion that one expects big haloes to 'form' later than small haloes, without distinguishing between the dynamical collapse or assembly of these haloes and the formation epoch of the stars in them. The observed downsizing is therefore frequently referred to in the literature as 'antihierarchical', and thus as posing a severe challenge to the standard model for structure formation. However, when comparing the histories of different haloes, the evolution may be interpreted as bottom-up or top-down depending on how 'formation' is defined.

The evolution of DM haloes has traditionally been studied through the histories of the *main progenitors* (Lacey & Cole 1993; Eisenstein & Loeb 1996; Nusser & Sheth 1999; Firmani & Avila-Reese 2000; van den Bosch 2002b, hereafter vdB02; Wechsler et al. 2002; Li, Mo & van den Bosch 2005). The main-progenitor assembly history is constructed by following back in time the most massive progenitor in each merger event. We term $M_{\rm main}(z)$ the main progenitor mass at redshift z. The corresponding formation redshift $z_{\rm main}$ of a halo of mass M_0 at $z = 0$ is commonly defined as the time at which the main progenitor contained one-half of today's mass, $M_{\rm main}(z_{\rm main}) = M_0/2$. According to this definition, more massive haloes indeed form later. The formation redshift of the main progenitor has been computed by Lacey & Cole (1993) based on the extended Press–Schechter (EPS) formalism, and the trend with mass has been confirmed for various cosmologies (see e.g. vdB02). This has also been tested using trees extracted from cosmological N-body simulations (Lacey & Cole 1994; Wechsler et al. 2002). We confirm this behaviour below using a new analytic estimation of the full time evolution of $M_{\rm main}(z)$, based on the EPS formalism itself without the need to construct merger-tree realizations.

However, the history of the main progenitor of a given halo does not represent the history of the whole population of progenitors in which the stars of a present-day halo have formed. Perhaps more directly relevant for the stellar population at any given epoch is the sum over the masses of *all* the virialized progenitors in that specific tree at that time, which we term $M_{\rm all}(z)$. If this summation is performed down to a zero minimum mass, we have by definition $M_{\rm all}(z) = M_0$. However, when a non-zero minimum mass $M_{\rm min}(z)$ is applied, the same for all haloes, we find a robust ADS behaviour.[1] We demonstrate this effect analytically based on the EPS formalism

[1] A similar point has been made in parallel by Mouri & Taniguchi (2006) using a very different methodology.

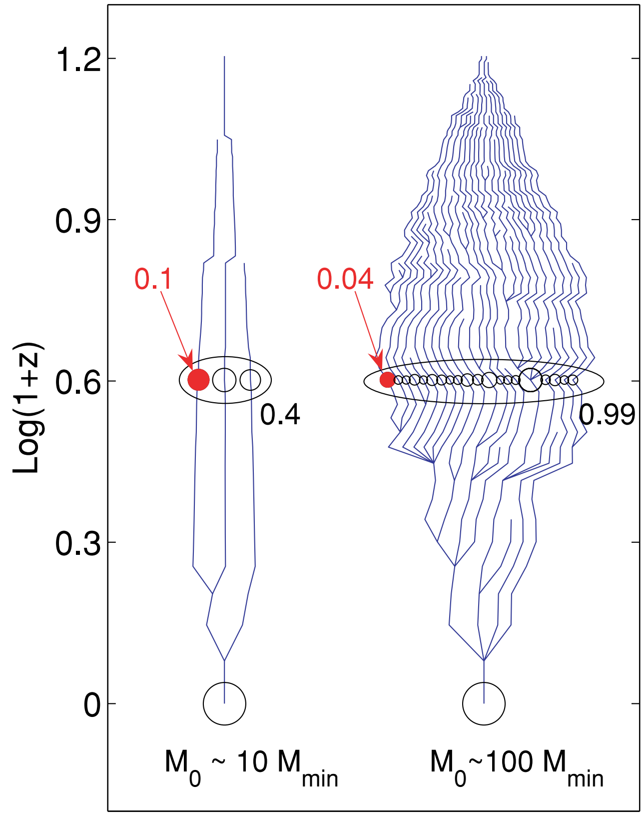

Figure 1. An illustration of the upsizing of $M_{\rm main}$ versus the downsizing of $M_{\rm all}$ in dark-halo merger trees. Compared are random trees drawn from the EPS probabilities for haloes of current masses $M_0 \sim 10$ and $\sim 100 M_{\rm min}$. The mass of the main progenitor versus the total mass in all the progenitors above $M_{\rm min}$ is shown at $z = 3$. The progenitors, of mass M, are marked by circles of sizes and spacings proportional to $(M/M_0)^{1/3}$. The values of $M_{\rm main}/M_0$ and $M_{\rm all}/M_0$ are indicated. The main progenitor, along the left-hand branch, is more massive in the less massive M_0, showing upsizing. The integrated mass in all the progenitors down to $M_{\rm min}$ is larger in the massive M_0, demonstrating 'downsizing'.

and confirm it using Monte Carlo EPS merger trees as well as trees extracted from N-body simulations. We prove that this phenomenon is valid for any realistic power-spectrum shape and for any choice of $M_{\rm min}(z)$, as long as it is the same for all haloes at a given time. We note that a similar trend has been found by Bower (1991) for an Einstein–deSitter cosmology and a power-law power spectrum.

The difference between $M_{\rm main}$ and $M_{\rm all}$ is illustrated in Fig. 1, which compares the $z = 3$ progenitors above a given $M_{\rm min}$ in random realizations of merger trees corresponding to current haloes of $M_0 \sim 10$ and $\sim 100 M_{\rm min}$. The downsizing behaviour for $M_{\rm all}$ is apparent, while for $M_{\rm main}$ the familiar opposite trend stands out. (We term this trend as 'upsizing'.) The average distributions of relative masses in $z = 3$ progenitors, derived using EPS (see below) for the same two values of M_0 as in Fig. 1, are shown in Fig. 2. The upsizing of $M_{\rm main}$ is indicated by the excess of massive progenitors for the smaller current halo. The downsizing of $M_{\rm all}$ is demonstrated by the excess of the overall integral down to $M_{\rm min}/M_0$ for the more massive current halo.

A realistic and necessary condition for star formation is that the gas is able to cool efficiently. This is only possible if the gas resides in a halo whose virial temperature exceeds a critical threshold of $T \sim 10^4$ K, above which atomic cooling becomes efficient. This

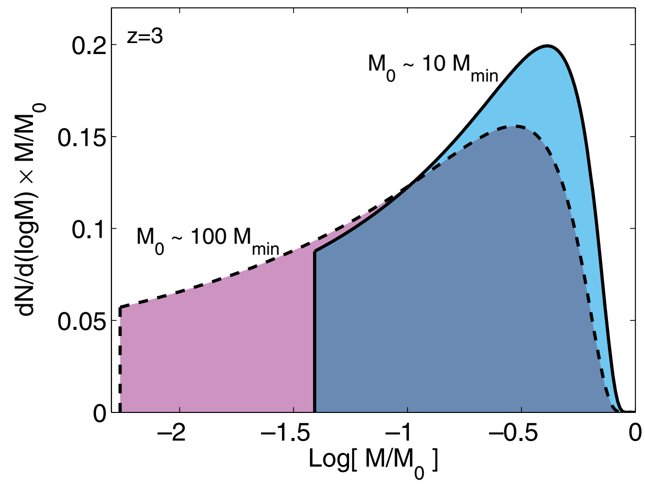

Figure 2. Upsizing of $M_{\rm main}$ versus downsizing of $M_{\rm all}$ in the distribution of mass in progenitors at $z = 3$. The area under each curve, from $\log(M/M_0)$ to 0, is the total mass in progenitors above M relative to M_0. The excess of mass in massive progenitors for the smaller current halo indicates upsizing of $M_{\rm main}$. The excess in total mass down to $M_{\rm min}/M_0$ for the more massive current halo demonstrates downsizing of $M_{\rm all}$.

provides a natural threshold $M_{\rm min}(z)$ for $M_{\rm all}(z)$. If star formation is of the maximum possible efficiency, namely if all the gas in haloes above $M_{\rm min}(z)$ turns into stars on a free-fall time-scale, then the ADS in the stellar population emerges naturally from the ADS of $M_{\rm all}(z)$.

In reality, however, the star formation rate is likely to be slowed down by a variety of baryonic processes, especially by 'feedback' effects. As a result, the star formation history may or may not maintain the ADS seeded by $M_{\rm all}(z)$ of the DM haloes. This should in principle be modelled by semi-analytic models (SAMs) of galaxy formation, which attempt to incorporate the baryonic physical processes in merger trees of DM haloes. Unfortunately, early SAMs failed to reproduce the ADS of ellipticals as we know it today (e.g. Baugh, Cole & Frenk 1996; Kauffmann 1996; Kauffmann & Charlot 1998; Thomas 1999; Thomas & Kauffmann 1999), probably due to an inadequate treatment of feedback effects. SAMs also failed to recover the similar global trend obeyed by blue-sequence galaxies in colour–magnitude diagrams (van den Bosch 2002a; Bell et al. 2003), thus highlighting the apparent discrepancy between theory and observation. However, more recent models (e.g. Bower et al. 2006; Cattaneo et al. 2006; Croton et al. 2006; De Lucia et al. 2006) do succeed in reproducing an ADS behaviour, largely because of an improved treatment of the feedback effects. The early SAMs only included supernova feedback, which is efficient in slowing down star formation preferentially in smaller galaxies below a virial velocity of $\sim$100 km s^{-1} (Dekel & Silk 1986). The problem is that this process only causes a *delay* in the star formation: the gas is only prevented from forming stars until the halo has grown sufficiently massive that supernova feedback is no longer efficient. Because this results in relatively late star formation, even in massive galaxies, the SAMs were unable to predict the correct stellar ages. The main success of the more modern SAMs is the inclusion of active galactic nucleus (AGN) feedback and shock heating physics, which causes a shutdown, rather than a delay, of star formation at relatively late times (e.g. Birnboim & Dekel 2003; Binney 2004; Scannapieco, Silk & Bouwens 2005; Cattaneo et al. 2006; Croton et al. 2006; Dekel & Birnboim 2006). Although the details of AGN feedback are still poorly understood, it has been argued that it is the main mechanism that explains the 'antihierarchical' nature of the relation between stellar mass and stellar age of galaxies.

However, we show below that the simulated star formation histories of elliptical galaxies (De Lucia et al. 2006) are qualitatively similar to the histories predicted by $M_{\rm all}(z)$ of DM haloes. This indicates that the roots of the observed ADS can be found already in the natural downsizing of the DM haloes. Apparently, the complex feedback processes affecting the star formation do not change the general trend and only provide fine-tuning to the ADS effect. We conclude that ADS should not be regarded as a surprising 'antihierarchical' phenomenon of complex gas physics – it is rather the most natural, expected behaviour in the hierarchical clustering scenario.

On the other hand, we find that the DST, as observed at relatively low redshifts, cannot be easily traced back to the bare properties of the DM merger trees. The mass distribution of late-type efficient star formers at late times must be strongly affected by feedback or other gas processes and therefore the modelling of this aspect of downsizing should involve more realistic star formation rates. We show that only when $M_{\rm min}(z)$ is properly increasing with redshift, possibly mimicking the required baryonic effects, the star formation rate associated with $M_{\rm all}(z)$ can be forced to a qualitative agreement with the observed DST.

This paper is organized as follows. In the following introductory section, Section 2, we spell out the relevant items from the EPS formalism and describe how we generate Monte Carlo merger trees that serve us as a reference when needed. In Section 3, we address the average $M_{\rm main}(z)$, derive an analytic approximation for it and confirm that it behaves opposite to downsizing. In Section 4, we study the average $M_{\rm all}(z)$, compute it analytically from the EPS formalism and demonstrate that it shows a robust ADS behaviour. We also study the mutual correlation between the formation times associated with $M_{\rm main}$ and $M_{\rm all}$. In Section 5, we compute the EPS formation rate of DM haloes of a given mass, and compare it with star formation histories in semi-analytic simulations and in observations. In Section 6, we address the DST of the SSFR as observed at different redshifts out to $z \sim 1$. In Section 7, we summarize our results and discuss them.

Throughout this paper, we use a flat ΛCDM cosmology, with the standard power spectrum $P(k) = kT^2(k)$. The transfer function (Bardeen et al. 1986) is

$$T(k) = \frac{\ln(1+2.34q)}{2.34q} \times [1 + 3.89q + (16.1q)^2 + (5.46q)^3 + (6.71q)^4]^{-1/4}. \tag{1}$$

Here, $q = k/\Gamma$, with k in hMpc^{-1}, and Γ is the power spectrum shape parameter (Sugiyama 1995)

$$\Gamma = \Omega_{\rm m} h \exp[-\Omega_{\rm b}(1 + \sqrt{2h}/\Omega_{\rm m})], \tag{2}$$

where $\Omega_{\rm b} = 0.044$ throughout the paper. Unless specifically stated otherwise, we use the standard cosmological parameters, with $\Omega_\Lambda = 0.7$, $\Omega_{\rm m} = 0.3$, $\sigma_8 = 1.0$ and $h = 0.7$. (Whenever we modify $\Omega_{\rm m}$ or h, we recompute Γ according to the above definition.)

2 EXTENDED PRESS–SCHECHTER THEORY

2.1 The formalism

In the standard model for structure formation, the initial density contrast $\delta(\boldsymbol{x}) = \rho(\boldsymbol{x})/\bar{\rho} - 1$ is considered to be a Gaussian random field, which is therefore completely specified by the power spectrum

$P(k)$. As long as $\delta \ll 1$, the growth of the perturbations is linear and $\delta(\boldsymbol{x}, t_2) = \delta(\boldsymbol{x}, t_1)\, D(t_2)/D(t_1)$, where $D(t)$ is the linear growth factor. Once $\delta(\boldsymbol{x})$ exceeds a critical threshold $\delta^0_{\rm crit}$, the perturbation starts to collapse to form a virialized object (halo). In the case of spherical collapse $\delta^0_{\rm crit} \simeq 1.68$. In what follows, we define δ_0 as the initial density contrast field linearly extrapolated to the present time. In terms of δ_0, regions that have collapsed to form virialized objects at redshift z are then associated with those regions for which $\delta_0 > \delta_c(z) \equiv \delta^0_{\rm crit}/D(z)$.

In order to assign masses to these collapsed regions, the Press–Schechter (PS) formalism considers the density contrast δ_0 smoothed with a spatial window function (filter) $W(r; R_{\rm f})$. Here, $R_{\rm f}$ is a characteristic size of the filter, which is used to compute a halo mass $M = \gamma_{\rm f} \bar{\rho} R^3_{\rm f}/3$, with $\bar{\rho}$ the mean mass density of the Universe and $\gamma_{\rm f}$ a geometrical factor that depends on the particular choice of filter. The *ansatz* of the PS formalism is that the fraction of mass that at redshift z is contained in haloes with masses greater than M is equal to two times the probability that the density contrast smoothed with $W(r; R_{\rm f})$ exceeds $\delta_c(z)$. This results in the well-known PS mass function for the comoving number density of haloes:

$$\frac{{\rm d}n}{{\rm d}\ln M}(M, z)\,{\rm d}M = \sqrt{\frac{2}{\pi}}\, \bar{\rho}\, \frac{\delta_c(z)}{\sigma^2(M)} \left|\frac{{\rm d}\sigma}{{\rm d}M}\right| \exp\left[-\frac{\delta_c^2(z)}{2\sigma^2(M)}\right] {\rm d}M \tag{3}$$

(Press & Schechter 1974). Here, $\sigma^2(M)$ is the mass variance of the smoothed density field given by

$$\sigma^2(M) = \frac{1}{2\pi^2} \int_0^\infty P(k)\, \widehat{W}^2(k; R_{\rm f})\, k^2\, {\rm d}k, \tag{4}$$

with $\widehat{W}(k; R_{\rm f})$ the Fourier transform of $W(r; R_{\rm f})$.

The EPS model developed by Bond et al. (1991) is based on the excursion set formalism. For each point, one constructs 'trajectories' $\delta(M)$ of the linear density contrast at that position as a function of the smoothing mass M. In what follows, we adopt the notation of Lacey & Cole (1993, hereafter LC93) and use the variables $S = \sigma^2(M)$ and $\omega = \delta_c(z)$ to label mass and redshift, respectively. In the limit $R_{\rm f} \rightarrow \infty$, one has that $S = \delta(S) = 0$, which can be considered the starting point of the trajectories. Increasing S corresponds to decreasing the filter mass M, and $\delta(S)$ starts to wander away from zero, executing a random walk (if the filter is a sharp k-space filter). The fraction of matter in collapsed objects in the mass interval M, $M + {\rm d}M$ at redshift z is now associated with the fraction of trajectories that have their *first upcrossing* through the barrier $\omega = \delta_c(z)$ in the interval S, $S + {\rm d}S$, which is given by

$$f(S, \omega)\, {\rm d}S = \frac{1}{\sqrt{2\pi}}\, \frac{\omega}{S^{3/2}}\, \exp\left(-\frac{\omega^2}{2S}\right) {\rm d}S \tag{5}$$

(Bond et al. 1991; Bower 1991; LC93). After conversion to number counting, this probability function yields the PS mass function of equation (3). Note that this approach does not suffer from the arbitrary factor 2 in the original PS approach.

Since for random walks, the upcrossing probabilities are independent of the path taken (i.e. the upcrossing is a Markov process), the probability for a changed ΔS in a time-step $\Delta\omega$ is simply given by equation (5) with S and ω replaced with ΔS and $\Delta\omega$, respectively. This allows one to immediately write down the *conditional* probability that a particle in a halo of mass M_2 at z_2 was embedded in a halo of mass M_1 at z_1 (with $z_1 > z_2$) as

$$P(S_1, \omega_1 | S_2, \omega_2)\, {\rm d}S_1 = f(S_1 - S_2, \omega_1 - \omega_2){\rm d}S_1$$
$$= \frac{1}{\sqrt{2\pi}}\, \frac{(\omega_1 - \omega_2)}{(S_1 - S_2)^{3/2}}\, \exp\left[-\frac{(\omega_1 - \omega_2)^2}{2(S_1 - S_2)}\right] {\rm d}S_1. \tag{6}$$

Converting from mass weighting to number weighting, one obtains the average number of progenitors at z_1 in the mass interval M_1, $M_1 + {\rm d}M_1$ which by redshift z_2 have merged to form a halo of mass M_2:

$$\frac{{\rm d}N}{{\rm d}M_1}(M_1, z_1 \,|\, M_2, z_2)\, {\rm d}M_1 = \frac{M_2}{M_1}\, P(S_1, \omega_1 | S_2, \omega_2) \left|\frac{{\rm d}S}{{\rm d}M}\right| {\rm d}M_1. \tag{7}$$

2.2 Constructing merger trees

The conditional mass function can be combined with Monte Carlo techniques to construct merger histories (also called merger trees) of DM haloes. If one wants to construct a set of progenitor masses for a given parent halo mass, one needs to obey two requirements. First, the *number* distribution of progenitor masses of many independent realizations needs to follow (7). Secondly, mass needs to be conserved, so that in each individual realization the sum of the progenitor masses is equal to the mass of the parent halo. In principle, this requirement for mass conservation implies that the probability for the mass of the nth progenitor needs to be conditional on the masses of the $n - 1$ progenitor haloes already drawn. Unfortunately, these conditional probability functions are unknown, and one has to resort to an approximate technique for the construction of merger trees.

The most widely adopted algorithm is the N-branch tree method with accretion developed by Somerville & Kolatt (1999, hereafter SK99). This method is more reliable than, for example, the binary-tree method of LC93. In particular, it ensures exact mass conservation and yields conditional mass functions that are in good agreement with direct predictions from EPS theory (i.e. the method is self-consistent).

The SK99 method works as follows. First, a value for ΔS is drawn from the mass-weighted probability function

$$f(\Delta S, \Delta\omega)\, {\rm d}\Delta S = \frac{1}{\sqrt{2\pi}}\, \frac{\Delta\omega}{\Delta S^{3/2}}\, \exp\left[-\frac{(\Delta\omega^2)}{2\Delta S}\right] {\rm d}\Delta S \tag{8}$$

(cf. equation 6). Here, $\Delta\omega$ is a measure for the time-step used in the merger tree, and is a free parameter (see below). The progenitor mass, $M_{\rm p}$, corresponding to ΔS follows from $\sigma^2(M_{\rm p}) = \sigma^2(M) + \Delta S$. With each new progenitor, it is checked whether the sum of the progenitor masses drawn thus far exceeds the mass of the parent, M. If this is the case, the progenitor is rejected and a new progenitor mass is drawn. Any progenitor with $M_{\rm p} < M_{\rm min}$ is added to the mass component $M_{\rm acc}$ that is considered to be accreted on to the parent in a smooth fashion. (That is, the formation history of these small mass progenitors is not followed further back in time.) Here, $M_{\rm min}$ is a free parameter that has to be chosen sufficiently small. This procedure is repeated until the total mass left, $M_{\rm left} = M - M_{\rm acc} - \sum M_{\rm p}$, is less than $M_{\rm min}$. This remaining mass is assigned to $M_{\rm acc}$, and one moves on to the next time-step.

As all other methods for constructing merger trees (e.g. LC93; Kauffmann & White 1993), the SK99 algorithm is only an approximation. In particular, it is based on the *mass*-weighted progenitor probability function (8), rather than on the *number* distribution (7), and mass conservation is enforced 'by hand' by rejecting progenitor masses that overflow the mass budget. Consequently, the number distribution of the first-drawn progenitor masses is different from that of the second-drawn progenitor masses, etc. Somewhat fortunately, the sum of these distributions closely matches the number distribution (7) of all progenitors, but only if sufficiently small time-steps $\Delta\omega$ are used (see SK99; vdB02). In principle, since the upcrossing of random walks through a boundary is a Markov process, the statistics of progenitor masses should be independent of the time-steps taken, indicating that the method is not perfectly justified. Consequently, not all statistics of the merger trees thus constructed are necessarily accurate, something that has to be kept in mind.

In this paper, we adopt a time-step of

$$\Delta\omega = \sqrt{\left|\frac{\mathrm{d}S}{\mathrm{d}M}\right| 10^{-3} M} \left[b + a \log_{10}\left(\frac{M}{M_{\mathrm{min}}}\right)\right]^{-1}, \tag{9}$$

where $a = 0.3$ and $b = 0.8$. As shown in SK99, this time-step yields number distributions of progenitor masses that are in good agreement with (7). The average number of progenitors per time-step is $\sim$1.5 for $10^9\ h^{-1}\,\mathrm{M}_\odot \leqslant M \leqslant 10^{14}\ h^{-1}\,\mathrm{M}_\odot$ and $M_{\mathrm{min}} = 10^8\ h^{-1}\,\mathrm{M}_\odot$.

3 GROWTH OF THE MAIN PROGENITOR

The full merger history of any individual DM halo is a complex structure containing a lot of information. It has therefore been customary to define a *main progenitor history*, sometimes termed *mass accretion history* (Firmani & Avila-Reese 2000; Wechsler et al. 2002; vdB02) or *mass assembly history* (Li et al. 2005), which restricts attention to the main 'trunk' of the merger tree. This main trunk is defined by following the branching of a merger tree back in time, and selecting at each branching point the most massive progenitor. We denote by $M_{\mathrm{main}}(z)$ the mass of this main progenitor as a function of redshift z. Note that with this definition, the main progenitor is not necessarily the most massive progenitor of its generation at a given time, even though it never accretes other haloes that are more massive than itself.

3.1 Analytical derivation

Using EPS merger trees and cosmological N-body simulations, vdB02 and Wechsler et al. (2002) have obtained simple fitting formulae for the main progenitor history. We show here that one can actually derive a useful analytical approximation for the average $\bar{M}_{\mathrm{main}}(z)$, defined at each redshift as the average mass of $M_{\mathrm{main}}(z)$ over an ensemble of merger trees. We derive it directly from the EPS formalism, without the need to construct Monte Carlo merger trees. As shown in the Appendix, $\bar{M}_{\mathrm{main}}(z)$ obeys the differential equation

$$\frac{\mathrm{d}\bar{M}_{\mathrm{main}}}{\mathrm{d}\omega} = -\sqrt{\frac{2}{\pi}}\frac{\bar{M}_{\mathrm{main}}}{\sqrt{S_q - S}}. \tag{10}$$

Here, $S = S(\bar{M}_{\mathrm{main}})$, $S_q = S(\bar{M}_{\mathrm{main}}/q)$ and the value of q is between 2 and a maximum value q_{max}. We show in the Appendix that the uncertainty in q is an intrinsic property of the EPS theory; different algorithms for constructing merger trees may correspond to different q within the allowed range. The maximum value, q_{max}, depends slightly on cosmology and mass. For example, q_{max} is between 2.1 and 2.3 for flat cosmogonies with Ω_{m} between 0.1 and 0.9 and halo masses between 10^8 and $10^{15}\ h^{-1}\,\mathrm{M}_\odot$.

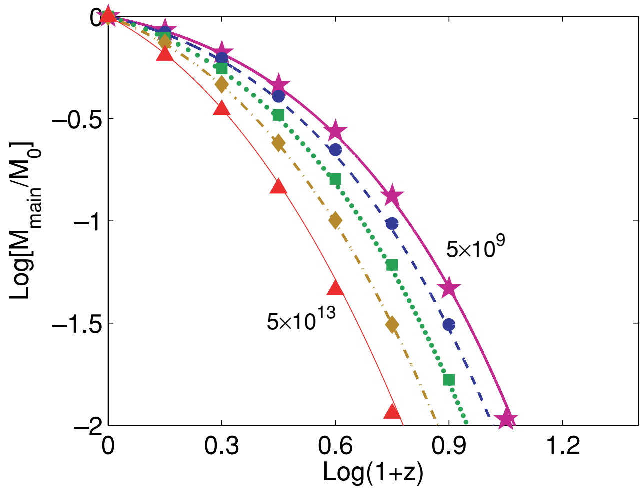

Figure 3. Growth of the main progenitor for haloes of different present-day masses. The mass $\bar{M}_{\mathrm{main}}(z)$ is the average at a fixed redshift z. The curves are normalized to match at $z = 0$. The halo masses, from top to bottom, range from 5×10^9 to $5 \times 10^{13}\ h^{-1}\,\mathrm{M}_\odot$ equally spaced in the log. The symbols refer to the averages over Monte Carlo merger trees, and the curves represent our analytic results. The upsizing of the main progenitor is obvious.

Solving the differential equation for $\bar{M}_{\mathrm{main}}$, we come up with a useful fitting formula:

$$\bar{M}_{\mathrm{main}}(z) = \frac{\Omega_{\mathrm{m}}}{\Gamma^3} F_q^{-1}\left\{\frac{g(32\Gamma)}{\sigma_8}[\omega(z) - \omega_0] + F_q\left(\frac{\Gamma^3}{\Omega_{\mathrm{m}}} M_0\right)\right\}. \tag{11}$$

Here, g and F_q are analytic fitting functions motivated by the shape of the power spectrum (see Appendix for their definition and range of accuracy). For the ΛCDM concordance cosmology, we find that the standard algorithm of SK99 for constructing random merger trees yields a $\bar{M}_{\mathrm{main}}(z)$ which is well fitted by equation (11) with $q = 2.2$. We therefore adopt this value below. Varying q between 2 and 2.3 (the maximum range allowed) gives rise to a relatively small change in $\bar{M}_{\mathrm{main}}$; near $\bar{M}_{\mathrm{main}} = 0.5M_0$ this change is $\sim$8 per cent.

Fig. 3 shows $\bar{M}_{\mathrm{main}}(z)/M_0$, the average, main progenitor history for haloes of different masses today, all normalized to today's mass. The figure compares our analytic estimate based on equation (11) with the averages over histories computed from Monte Carlo merger-tree realizations described in Section 2.2. We see that the analytic estimate reproduces the results from the realizations quite well, although there is a slight mismatch at high z. This difference may either reflect the allowed intrinsic uncertainty within the EPS formalism or be due to other inaccuracies in the SK99 algorithm used to construct the trees.

3.2 Archaeological upsizing

We see in Fig. 3 that the average growth curve of the main progenitor is shifted towards later times in more massive haloes, implying the opposite of downsizing, termed here as upsizing. One way to quantify the downsizing behaviour is via the quantity

$$D_{\mathrm{main}}(z\,|\,z_0, M_0) \equiv \frac{\mathrm{d}}{\mathrm{d}M_0}\left[\frac{\bar{M}_{\mathrm{main}}(z)}{M_0}\right]. \tag{12}$$

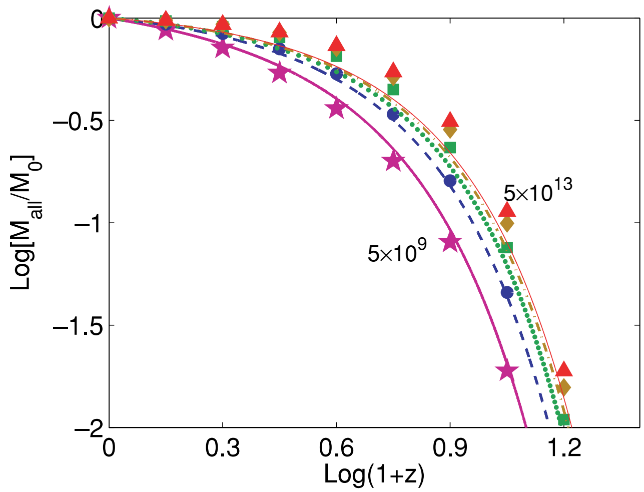

Figure 4. Growth of the total mass in all the progenitors, $\bar{M}_{\rm all}(z)$, for haloes of different present-day masses. The minimum progenitor mass is $\sim 10^9\,{\rm M}_\odot$, specified in equation (20) as a function of redshift. The masses, curves and symbols are the same as in Fig. 3. A downsizing behaviour is clearly seen. It is more pronounced at small masses which are closer to $M_{\rm min}$.

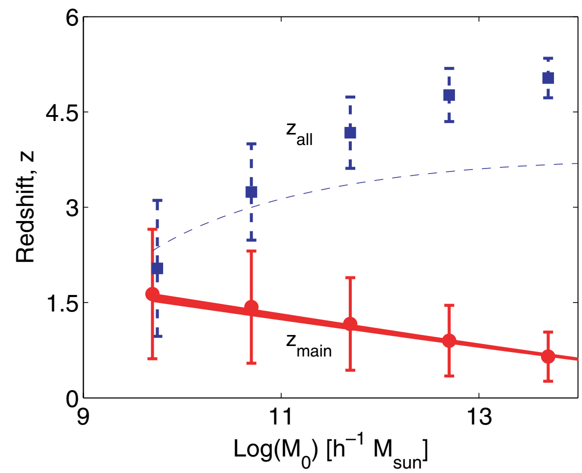

Figure 5. Formation redshifts, when the mass was one-half of today's mass, for the main progenitor ($\bar{z}_{\rm main}$, solid lines, circles) and for all the progenitors ($\bar{z}_{\rm all}$, dashed lines, squares) versus today's halo mass. The symbols and error bars refer to an ensemble of random EPS merger trees. The thickness of the $\bar{z}_{\rm main}$ curve refers to the allowed range obtained by varying q between 2 and $q_{\rm max}$ in equation (15). The dashed line is the theoretical prediction (23) for $\bar{z}_{\rm all}$. $z_{\rm main}$ shows upsizing while $z_{\rm all}$ shows downsizing.

Positive values of $D_{\rm main}$ mark an ADS behaviour, negative values refer to upsizing and $|D_{\rm main}|$ measures the strength of the effect. As is clear from Fig. 3, $D_{\rm main}(z) < 0$ at all z, indicating that the main progenitor histories of DM haloes reveal upsizing.

Is this upsizing a generic feature of $\bar{M}_{\rm main}(z)$? To answer this, we write the average main progenitor mass of a halo of mass M_0 a small time-step $\Delta\omega$ ago as

$$\frac{\bar{M}_{\rm main}(\Delta\omega)}{M_0} = \int_0^{S_q - S_0} f(\Delta S, \Delta\omega)\,{\rm d}\Delta S \tag{13}$$

(see Appendix). Differentiating with respect to M_0 while keeping $\Delta\omega$ fixed yields the ADS strength

$$D_{\rm main}(z\,|\,z_0, M_0) = f(S_q - S_0, \Delta\omega)\left[\frac{1}{q}\frac{{\rm d}S}{{\rm d}M}(M_0/q) - \frac{{\rm d}S}{{\rm d}M}(M_0)\right]. \tag{14}$$

Whether this is negative or not depends on the shape of $S(M)$. For a self-similar power spectrum, $S \propto M^{-\alpha}$, we have that $D_{\rm main} < 0$ as long as $\alpha > 0$. We have also verified numerically that $D_{\rm main} < 0$ for the standard ΛCDM power spectrum at all masses. While the above expression for $D_{\rm main}$ is valid only for small $\Delta\omega$, its sign is the same at all z. A more accurate expression for $D_{\rm main}$ at any z can be obtained by differentiating equation (11).

3.3 Assembly time of the main progenitor

Following numerous other studies (see Section 1), we define the assembly redshift $z_{\rm main}$ of a halo of mass M_0 at time ω_0 according to $M_{\rm main}(z_{\rm main}) = M_0/2$. Using equation (11), we obtain

$$\begin{aligned}\bar{\omega}_{\rm main} &\equiv \omega(\bar{z}_{\rm main})\\ &= \omega_0 + \frac{\sigma_8}{g(32\Gamma)}\left[F_q\left(\frac{\Gamma^3}{\Omega_{\rm m}}\frac{M_0}{2}\right) - F_q\left(\frac{\Gamma^3}{\Omega_{\rm m}}M_0\right)\right].\end{aligned} \tag{15}$$

In the case of scale-free initial conditions, where the power spectrum is a pure power law, $P(k) \propto k^n$, we have that $S \propto M^{-\alpha}$ with $\alpha = (n+3)/3$. In this case, the expression simplifies to

$$\bar{\omega}_{\rm main} = \omega_0 + \frac{\sqrt{2\pi(q^\alpha - 1)}}{\alpha}(\sqrt{S_q} - \sqrt{S_0}). \tag{16}$$

We note that Lacey & Cole (1993) computed a related expression for the average assembly redshift of the main progenitor (see the Appendix for more details).

Fig. 5 shows the average assembly redshift of the main progenitor, $\bar{z}_{\rm main}$, as a function of the present-day halo mass, for the ΛCDM concordance cosmology. The thickness of the curve corresponds to the allowed range of intrinsic uncertainty in q in equation (15), as computed in the Appendix. The ADS strength, $D_{\rm main}$, associated with the slope of $\bar{z}_{\rm main}(M)$, does not change significantly with halo mass. The theoretical EPS curve shows an excellent agreement with the $\bar{z}_{\rm main}$ obtained from an ensemble of random EPS merger histories (circles with error bars). The error bars correspond to the standard deviation in $z_{\rm main}$ over the individual merger trees.

Fig. 5 demonstrates again the upsizing behaviour of the main progenitor. This has been one of the reasons for interpreting the observed downsizing as 'antihierarchical'.

The distribution of $z_{\rm main}$ in our ensemble of EPS merger trees is plotted in Fig. 6 for three different masses. One of them is compared to the theoretical prediction by LC93,

$$Q(z) = -\frac{\rm d}{{\rm d}z}\int_{S_0}^{S_2}\frac{M_0}{M}f[S - S_0, \omega(z) - \omega_0]\,{\rm d}S, \tag{17}$$

where f is as defined in equation (5). As discussed in the Appendix, the theoretical distribution agrees with the random realizations at low z, and any deviations are due to the limitations of the SK99 algorithm used.

4 GROWTH OF ALL THE PROGENITORS

$M_{\rm main}(z)$ defined above only describes the mass growth history of the main trunk of the full merger tree. It is unlikely, however, that this is an honest estimator of the star formation histories of the associated galaxies. After all, star formation can occur in *all* progenitors that obey the necessary physical conditions, and is not restricted to the *main* progenitor. Since gas needs to cool before it can form stars, and since the cooling time is primarily a function of halo mass and redshift, we assume that star formation occurs in haloes with

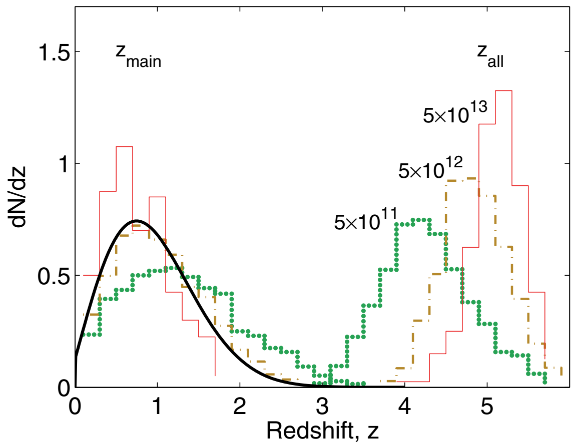

Figure 6. The distribution of $z_{\rm main}$ and $z_{\rm all}$ for different halo masses. Halo masses are 5×10^{11}, 5×10^{12} and $5 \times 10^{13}\,h^{-1}\,{\rm M}_\odot$ (dotted, dash–dotted and solid lines). The solid thick line is the theoretical prediction for the distribution of $z_{\rm main}$, equation (17), for a halo mass of $5 \times 10^{12}\,h^{-1}\,{\rm M}_\odot$. The minimum progenitor mass is $\sim 10^9\,{\rm M}_\odot$, specified in equation (20) as a function of redshift.

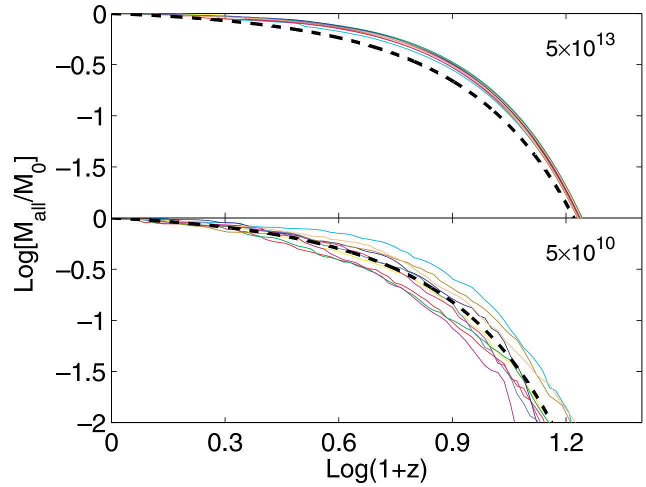

Figure 7. Individual realizations of all-progenitor histories (thin solid curves) compared to the average at fixed z as calculated analytically (thick dashed curve). The curves are all normalized to M_0 at $z = 0$. The upper and lower panels are for $M_0 = 5 \times 10^{13}$ and $5 \times 10^{10}\,h^{-1}\,{\rm M}_\odot$, respectively. $M_{\rm min}$ is specified in equation (20).

a mass above a threshold mass, $M_{\rm min}(z)$. This prompts us to define the formation history $M_{\rm all}(z)$ of a present-day DM halo as the sum of the masses of all progenitors that obey this condition. Supporting evidence for the possible success of such a model comes from the finding that the integral of $M_{\rm all}(z)$ over the entire present-day halo mass function provides a useful backbone for understanding the observed, universal star formation history (Hernquist & Springel 2003).

4.1 Analytical derivation

The construction of $M_{\rm all}(z)$ for individual DM haloes requires a full merger tree, with a mass resolution that exceeds $M_{\rm min}(z)$. However, the formation history of a halo of mass M_0, averaged over many merger trees per each redshift z, can be derived straightforwardly from the EPS formalism. It should equal the integral over the progenitor mass function in the range $M = M_{\rm min}(z)$ to M_0:

$$\bar{M}_{\rm all}(z) = M_0 \int_{M_{\rm min}(z)}^{M_0} P(S, \omega \,|\, S_0, \omega_0) \left| \frac{{\rm d}S}{{\rm d}M} \right| {\rm d}M, \tag{18}$$

where $P(S, \omega\,|S_0, \omega_0)$ is as defined in equation (6). Performing the integral, we obtain

$$\frac{\bar{M}_{\rm all}(z)}{M_0} = 1 - {\rm erf}\left[\frac{\omega(z) - \omega_0}{\sqrt{2S_{\rm min}(z) - 2S_0}} \right] \tag{19}$$

where $S_{\rm min}(z) \equiv S[M_{\rm min}(z)]$. Note that $\bar{M}_{\rm all}(z)/M_0$ depends on M_0 through S_0, so that equation (19) cannot be written in an explicit form.

We see that for a given cosmology, the average formation history of a halo of mass M_0 is completely specified by $M_{\rm min}(z)$. As a first attempt, we associate $M_{\rm min}$ with the halo mass that corresponds to a virial temperature of $T_{\rm vir} = 10^4$ K, the temperature above which atomic gas is able to cool and subsequently form stars. For a completely ionized, primordial gas, this yields

$$M_{\rm min}(z) = 1.52 \times 10^9 h^{-1}\,{\rm M}\odot \left(\frac{\Delta_{\rm vir}}{101} \right)^{-1/2} \left[\frac{H(z)}{H_0} \right]^{-1}, \tag{20}$$

where $\Delta_{\rm vir}(z)$ is the average overdensity of a virialized halo at redshift z relative to the critical density at that redshift (Bryan & Norman 1998) and $H(z)$ is the Hubble parameter. Unless specifically stated otherwise, we use this minimum threshold mass in what follows.

The lines in Fig. 4 show $\bar{M}_{\rm all}(z)$ for several halo masses based on equation (19). We now see that when 'formation' is defined by $\bar{M}_{\rm all}(z)$ we obtain ADS, with more massive haloes forming *earlier*. Also plotted in Fig. 4 are the results of the merger trees (symbols). We see that while there is a fair, qualitative agreement between the histories extracted from the Monte Carlo realizations and the exact EPS predictions, the level of agreement becomes progressively worse for more massive haloes (relative to $M_{\rm min}$). The merger trees predict an earlier formation time than what follows directly from EPS. A similar behaviour has been noted by SK99 (their fig. 7), when comparing the empirical total mass contained in haloes above a minimum mass to the theoretical value. These deviations arise from the approximations made in the algorithm for constructing the Monte Carlo merger trees (see Discussion in Section 2.2).

Fig. 7 shows the $M_{\rm all}(z)$ histories of individual haloes, obtained from Monte Carlo merger-tree realizations (thin lines), compared to the average formation history $\bar{M}_{\rm all}(z)$, calculated from equation (19) (thick dashed line). The scatter is higher for lower mass haloes. This can be crudely understood as a Poisson noise associated with $N_{\rm all}$, the number of progenitors above $M_{\rm min}$ at every given redshift. For the massive halo, $M_0 = 5 \times 10^{13}\,h^{-1}\,{\rm M}_\odot$, $N_{\rm all}$ is indeed quite large at all redshifts, leading to a small scatter. For the less massive halo, $M_0 = 5 \times 10^{10}\,h^{-1}\,{\rm M}_\odot$, we have $N_{\rm all} < 20$ at all redshifts, which results in a larger scatter.

4.2 Archaeological downsizing

The all-progenitor histories $M_{\rm all}(z)$ depend on the definition of the threshold mass $M_{\rm min}(z)$. Here, we investigate the necessary conditions for these threshold masses in order for $\bar{M}_{\rm all}(z)$ to reveal ADS. Similar to what was done in Section 3.2, we define the 'downsizing strength', $D_{\rm all}$, as the derivative of $\bar{M}_{\rm all}/M_0$ with respect to M_0. In order to study the M_0 dependence, we rewrite equation (18) using different variables,

$$\frac{\bar{M}_{\rm all}(\omega)}{M_0} = \int_0^{S_{\rm min}-S_0} f(\Delta S, \omega - \omega_0) {\rm d}\Delta S, \tag{21}$$

where the function f is defined as in equation (5). This enables us to differentiate $M_{\rm all}/M_0$ with respect to M_0, while keeping ω fixed, which yields

$$D_{\rm all}(\omega \mid \omega_0, M_0) = -f(S_{\rm min} - S_0, \omega - \omega_0) \frac{{\rm d}S}{{\rm d}M}(M_0) > 0. \tag{22}$$

Since f is a probability function, and ${\rm d}S/{\rm d}M < 0$ for all M, we have that $D_{\rm all}$ is always positive. This implies that ADS occurs for any choice of the threshold masses $M_{\rm min}(z)$ and for any cosmological power spectrum of fluctuations. The only assumptions used are (i) that the threshold is global, i.e. that $M_{\rm min}$ does not depend on the specific halo mass M_0, and (ii) that the excursion-set trajectories are Markovian, which allows the change of variables leading from equation (18) to (21). Note that the downsizing aspect of $\bar{M}_{\rm all}(z)$ does not depend on the actual shape of f, which implies that ADS will occur for non-Gaussian density fluctuation fields as well.

The opposite effect of upsizing could in principle occur if the Markovian assumption of the EPS random walks breaks down, so that the mass-weighted probability distribution $P(S, \omega \mid S_0, \omega_0)$ depends on S_0 rather than being a function of $S - S_0$ only. An additional requirement in this case is that the probability has a higher contribution from the low-mass end for larger M_0. Therefore, the Markovian nature of the random walks is a sufficient, but not a necessary, condition for ADS to occur.

4.3 Formation time of all progenitors

Following the definition of assembly redshift, we define the formation redshift of DM haloes, $z_{\rm all}$, by $M_{\rm all}(z_{\rm all}) = M_0/2$. Using equation (19), we obtain

$$\bar{\omega}_{\rm all} \equiv \omega(\bar{z}_{\rm all}) = \omega_0 + \beta\sqrt{S_{\rm min} - S_0}, \tag{23}$$

where $\beta = \sqrt{2}/{\rm erf}(1/2) \simeq 0.6745$ (see also Bower 1991). The dashed curve in Fig. 5 shows $z_{\rm all}$ as a function of halo mass computed using equation (23). The solid square with error bars represents the average and scatter as obtained from a large ensemble of EPS merger trees. Note that these deviate significantly from the direct theoretical EPS prediction, especially at large M_0. This is in stark contrast to the case of $z_{\rm main}(M_0)$, where the merger-tree results agree well with the direct theoretical predictions. This suggests that the discrepancy in $z_{\rm all}(M_0)$ must originate in the statistics of smaller progenitors with masses $< M_0/2$. As shown by SK99, the N-branch tree method with accretion used for the construction of the EPS merger trees slightly overpredicts the number of small progenitors at high redshifts. Fig. 5 shows that this can have a significant impact on $z_{\rm all}$; consequently, SAMs for galaxy formation that are based on such EPS merger trees might actually overestimate the star formation rates at high redshifts.

For haloes with $M_0 \gg M_{\rm min}$, we have that $z_{\rm all} > z_{\rm main}$: typically the progenitors of a massive halo will have grown sufficiently massive to allow for star formation much before the final halo has assembled half its present-day mass into a single halo. Note that $z_{\rm all} - z_{\rm main}$ decreases with decreasing halo mass. When $M_0 \simeq 2M_{\rm min}$, we have that $z_{\rm all} = z_{\rm main}$, by definition, while $z_{\rm all} < z_{\rm main}$ for haloes with $M_{\rm min} < M_0 < 2M_{\rm min}$. Finally, for haloes with $M_0 < M_{\rm min}$ the formation redshift $z_{\rm all}$ is not defined. This systematic increase of $z_{\rm all} - z_{\rm main}$ with increasing halo mass may have interesting implications for galaxy formation, as it provides a very natural means to break the self-similarity between haloes of different masses, and their associated galaxies.

Although dynamical friction may delay the merging of galaxies with respect to the epoch at which their host haloes merged, to first order we may associate $z_{\rm main}$ with the redshift below which the haloes and their associated galaxies no longer experience major mergers (i.e. below $z_{\rm main}$ the main progenitor never merges with another halo of similar mass). In massive haloes, with $M_0 \gg M_{\rm min}$, we expect that the majority of the stars have already formed much before these last major mergers, and this majority of the stars will thus have experienced one or more major mergers since their formation. Consequently, the majority of the stars are most likely to reside in a spheroidal component, and the galaxy is an early-type with relatively old stars. Contrary, in low-mass haloes, most of the progenitor haloes that are being accreted by the main progenitor at $z < z_{\rm main}$ will have masses $M < M_{\rm min}$, and will, thus, not have formed stars. The gas associated with these progenitors can only start to form stars once they become part of the main progenitor: star formation and galaxy assembly occur virtually hand in hand, with the stars being born in situ in what is to become the final galaxy at $z = 0$. Since the system has not undergone a major merger since roughly half the stars formed, the system is likely to resemble a disc galaxy.

Although this is clearly severely oversimplified, it is interesting that some of the most pronounced scaling relations of galaxies, namely the relations between halo mass, stellar age and galaxy morphology, may well have their direct origin in the backbone of halo formation histories combined with a simple halo mass threshold for star formation.

Finally, Fig. 6 shows the distribution of $z_{\rm all}$ for haloes of different masses, as obtained from our EPS merger trees. Note that the scatter in $z_{\rm all}$ is smaller for more massive haloes, as expected from the Poisson statistics discussed in Section 4.1.

4.4 Comparison with *N*-body simulations

While the merger trees analysed thus far are based on the EPS formalism, one can alternatively extract merger trees from cosmological N-body simulations. Here, the gravitational dynamics are more accurate, limited only by numerical resolution effects. However, it should be kept in mind that the identification of virialized haloes, and especially connecting them to construct merger trees, is a non-trivial enterprise involving several significant uncertainties.

We compute $\bar{M}_{\rm all}(z)$ from merger trees extracted from a ΛCDM cosmological N-body simulation kindly provided by Risa Wechsler. The simulation followed the trajectories of 256^3 CDM particles within a cubic, periodic box of comoving size $60\,h^{-1}$ Mpc from redshift $z = 40$ to the present. The particle mass is $1.1 \times 10^9\,h^{-1}\,{\rm M}_\odot$, and the minimum halo mass dictated by the resolution is $2.2 \times 10^{10}\,h^{-1}\,{\rm M}_\odot$ (see Wechsler et al. 2002, for details). For the construction of $\bar{M}_{\rm all}(z)$, we impose $M_{\rm min}$ values of 5×10^{10} and $5 \times 10^{11}\,h^{-1}\,{\rm M}_\odot$, and we compare the resulting, average formation histories to those computed from the EPS formalism using the same threshold masses. The results are shown in Fig. 8, where symbols correspond to the formation histories extracted from the N-body simulations, while the lines show the direct, theoretical predictions based on the EPS formalism (equation 19). Overall, the agreement is very satisfactory, although the N-body simulations predict a somewhat later formation when $M_{\rm min} \ll M_0$. Note that the EPS *merger trees* yield formation times that are *earlier* with respect to the analytical formula (Fig. 4). Thus, the difference between N-body simulations and EPS merger trees is larger than the difference between the N-body simulations and equation (19). Despite these discrepancies, the N-body results clearly confirm the EPS prediction that $M_{\rm all}$ of more massive haloes grows earlier. We therefore conclude that

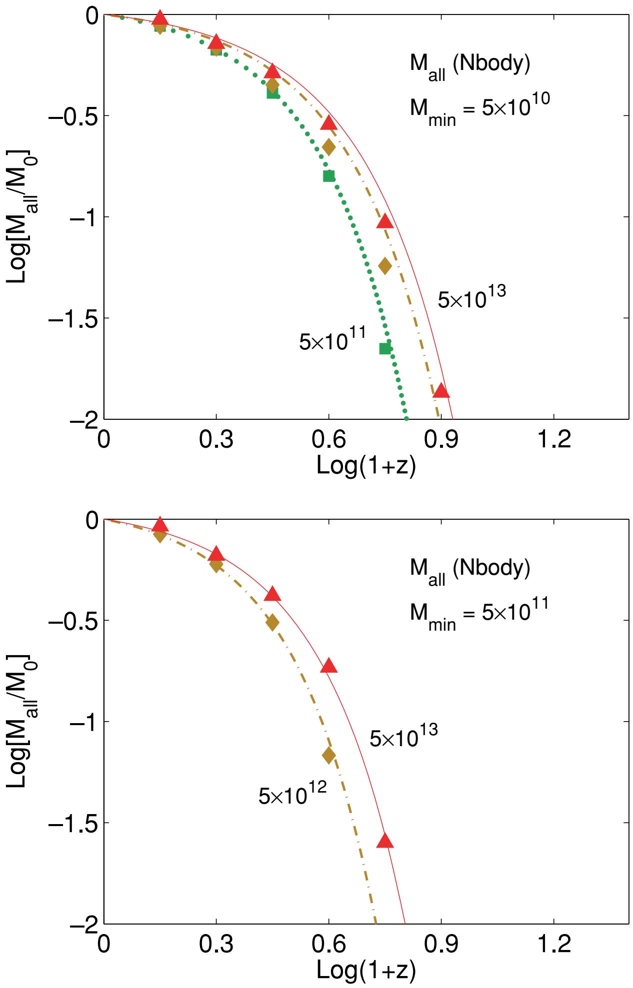

Figure 8. All-progenitor histories drawn from N-body simulations (symbols) compared to the EPS predictions (curves). The imposed minimum mass is $M_{\rm min} = 5 \times 10^{10}$ and 5×10^{11} $\rm M_{\odot}$ in the top and bottom panels, respectively. The mass bins in log mass are [11.62, 11.78], [12.48, 13.00], [13.48, 14.00] where mass units are h^{-1} $\rm M_{\odot}$. The number of haloes within each bin is 479, 205 and 23, respectively. The EPS theoretical curves corresponding to each mass bin are averages over the same distribution of masses.

the ADS aspect of $M_{\rm all}$ is not an artefact of the EPS approximation, but is a generic property of DM merger trees.

4.5 The correlation between formation time and assembly time

Since $z_{\rm all}$ increases with increasing halo mass (ADS), while $z_{\rm main}$ decreases ('upsizing'), we have that $z_{\rm all}$ and $z_{\rm main}$ are anticorrelated when considering haloes of different masses. But what about the relation between $z_{\rm all}$ and $z_{\rm main}$ for haloes of a fixed mass?

Fig. 9 shows the correlation between $z_{\rm all}$ and $z_{\rm main}$ for haloes of given masses, with $M_{\rm min} = 5 \times 10^{10}$. Results are shown for both the numerical simulations (solid dots) and EPS merger trees (contours). For a $5 \times 10^{11}\, h^{-1}$ $\rm M_{\odot}$ halo, the number of progenitors is small, and the full merger tree is not much more than the main trunk. As a result, the values of $z_{\rm all}$ and $z_{\rm main}$ are not very different and they exhibit a rather strong correlation. When the mass gets larger, the scatter in $z_{\rm all}$ tends to zero while the scatter in $z_{\rm main}$ remains large. Consequently, the correlation strength between $z_{\rm main}$ and $z_{\rm all}$ at fixed halo mass vanishes at large M_0.

This has important implications. Using a large numerical simulation, Gao, Springel & White (2005) and Harker et al. (2006) have found a positive correlation between $z_{\rm main}$ and the environment density: i.e. haloes in an overdense region assemble earlier than haloes of the same mass in an underdense region. If galaxy properties, such as stellar age, are correlated with $z_{\rm main}$, this means that haloes of a given mass host galaxies with different properties, depending on their large-scale environment. The results shown here suggest that this may be the case for relatively low mass haloes with $M_0 \simeq M_{\rm min}$, since these systems reveal a positive correlation between $z_{\rm main}$ and $z_{\rm all}$. In more massive haloes, however, with $M_0 \gg M_{\rm min}$, no such correlation is present, suggesting that the correlation between $z_{\rm main}$ and environment will not create a similar correlation between stellar age and environment.

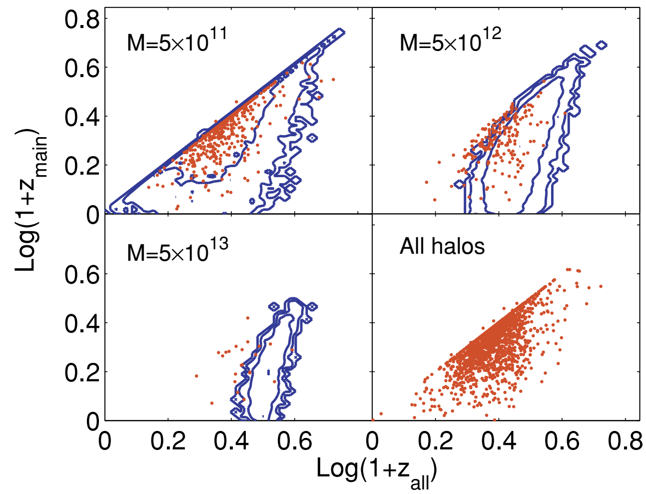

Figure 9. Correlations between $z_{\rm main}$ and $z_{\rm all}$ for random merger trees with the same final mass. The contours, equally spaced in the log, refer to the joint distribution from the EPS random merger trees. The minimum mass is $M_{\rm min} = 5 \times 10^{10}$. The points are from N-body merger trees, with the same mass bins as in Fig. 8.

The positive correlation between $z_{\rm main}$ and $z_{\rm all}$ at fixed mass arises from their dependence on the merger-tree properties at low redshifts. For example, assume that the merger tree for some halo is such that the mass at $z = 0.5$ is the same as at $z = 0$. In this case, we can use the analytical expressions for $z_{\rm all}$ and $z_{\rm main}$ starting at $z_0 = 0.5$, and not at $z_0 = 0$. The corresponding $z_{\rm main}$ and $z_{\rm all}$ will refer to $z_0 = 0.5$, so both will be delayed by the same amount of time, thus establishing a positive correlation.

When we increase the halo mass, the ratio $\bar{M}_{\rm main}(z)/\bar{M}_{\rm all}(z)$ decreases. (This is true for any specific redshift z.) This implies that the fraction of mass incorporated in the main trunk is smaller, and as a result, there is more mass left in progenitors that belong to other branches. The scatter in $\bar{M}_{\rm all}$ comes from all the tree branches, where each branch contributes its own random behaviour. When $\bar{M}_{\rm main}(z)$ is small with respect to $\bar{M}_{\rm all}(z)$, most of the contribution to the scatter in $\bar{M}_{\rm all}$ comes from branches other than the main. This explains why the correlation between $z_{\rm all}$ and $z_{\rm main}$ gets poorer for high halo mass.

5 HALO FORMATION RATES

We define the halo formation rate as the rate of change in $M_{\rm all}$. Using equation (19), this can be written as

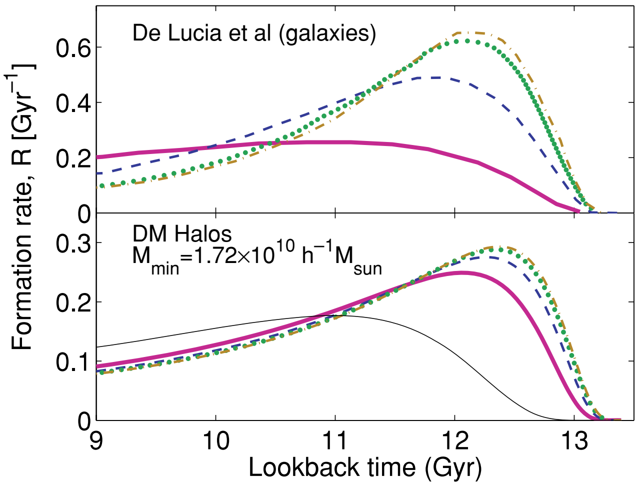

Figure 10. Simulated star formation rate versus EPS halo formation rate R for different halo masses. Top panel: mean SSFR of elliptical galaxies taken from the SAM of De Lucia et al. (2006). Galaxies are binned by their halo mass at $z = 0$. Bottom panel: maximum SFR as implied by our simplified model, namely R of equation (24), for different halo masses at $z = 0$. The curves in the two panels refer to halo masses of 10^{12}, 10^{13}, 10^{14} and 10^{15} $\mathrm{M}_{\odot}$ (solid, dashed, dotted, dash–dotted lines, respectively). $M_{\min}$ is $1.72 \times 10^{10}\, h^{-1}\, \mathrm{M}_{\odot}$, the minimum halo mass in De Lucia et al. (2006). In the lower panel, we add a curve for a halo mass of 10^{12} $\mathrm{M}_{\odot}$ with $M_{\min}$ set to 10^{11} $\mathrm{M}_{\odot}$ (thin solid line), as an example for the halo formation rate when $M_{\min}$ is only one order of magnitude below the halo mass.

$$R(\omega \,|\, \omega_0, M_0) \equiv \frac{\mathrm{d}}{\mathrm{d}t}\left[\frac{M_{\mathrm{all}}(\omega)}{M_0}\right]$$
$$= -\sqrt{\frac{2}{\pi}}\frac{1}{\sqrt{S_{\min} - S_0}} \exp\left[-\frac{(\omega-\omega_0)^2}{2S_{\min} - 2S_0}\right]\frac{\mathrm{d}\omega}{\mathrm{d}t}. \qquad (24)$$

If we make the naive assumption that all the baryonic mass inside haloes with $M > M_{\min}$ forms stars instantaneously, then this rate reflects the star formation history of galaxies that at time ω_0 are located in a halo of mass M_0: these formation rates basically reflect the maximum possible star-formation efficiency.

The upper panel of Fig. 10 shows the star formation histories of elliptical galaxies as a function of the mass of the halo in which these galaxies are located at $z = 0$, from the semi-analytic simulations of De Lucia et al. (2006, their fig. 3). Note that this model predicts that ellipticals in more massive haloes formed their stars earlier, and over a shorter period of time, in good, qualitative agreement with the observational data of Thomas et al. (2005) and Nelan et al. (2005). The lower panel of Fig. 10 shows the corresponding formation rates of the DM haloes, as defined by equation (24). Here, we have adopted the same cosmological parameters as in De Lucia et al. (i.e. $\Omega_\Lambda = 0.75$, $\Omega_{\mathrm{m}} = 0.25$, $\sigma_8 = 0.9$, $h = 0.73$) and we have used a constant threshold mass of $M_{\min} = 1.72 \times 10^{10}\, h^{-1}\, \mathrm{M}_{\odot}$, corresponding to the mass resolution of the numerical simulation used by these authors.

The formation rates of DM haloes, as seen in Fig. 10, reveal a qualitatively similar ADS behaviour as for elliptical galaxies in the SAM of De Lucia et al. (2006) and in the observational data (e.g. Thomas et al. 2005). Although the agreement is extremely good for the massive haloes, the SAM predicts a significantly later formation in lower mass haloes, indicating that the downsizing strength is larger in the SAM. This highlights the crudeness of our simplified model for star formation, while assumes that stars form instantaneously as soon as the halo mass exceeds $M_{\min}$. The comparison with the SAM suggests that this is a fairly accurate assumption in massive haloes. In low-mass haloes, however, the baryonic feedback processes modelled in the SAM must have caused a significant delay in the formation of the stars. Indeed, the efficiency of supernova feedback to cause such a delay is larger in lower mass haloes (Dekel & Silk 1986). In principle, we can increase the downsizing strength for the DM haloes by increasing $M_{\min}$. For example, the thin solid line plots the formation rates for a halo of 10^{12} $\mathrm{M}_{\odot}$ but with a higher $M_{\min}$ of 10^{11} $\mathrm{M}_{\odot}$. This brings the formation rates in better agreement with the SSFR of elliptical galaxies in haloes of 10^{12} $\mathrm{M}_{\odot}$ in the SAM. Thus, one may mimic the delays in star formation due to supernova feedback effects by an increase in the star formation threshold mass $M_{\min}$, even though we do not necessarily consider this very physical. We conclude that the ADS in galaxies has its natural origin in the ADS of M_{all}, while the baryonic physics associated with cooling, star formation and feedback merely cause the shifting and stretching of the relative formation histories. The main trend with halo mass, however, simply relates to the DM formation histories.

We define the mean formation epoch of a DM halo as

$$\omega_R \equiv \frac{\int_0^{t_0} R(\omega)\omega \mathrm{d}t}{\int_0^{t_0} R(\omega)\mathrm{d}t}. \qquad (25)$$

If, for simplicity, we keep the star formation threshold mass constant, i.e. $M_{\min}(z) = M_{\min}$, then this reduces to

$$\omega_R = \omega_0 + \sqrt{\frac{2}{\pi}(S_{\min} - S_0)}, \qquad (26)$$

where we have used the fact that the denominator of equation (25) is equal to unity. Note that this mean formation epoch is very similar to $\bar{\omega}_{\mathrm{all}}$ of equation (23), but with $\beta \simeq 0.67$ replaced by $\sqrt{2/\pi} \simeq 0.8$.

Fig. 11 compares our analytic estimates for the mean formation epoch of DM haloes to the star formation histories deduced from nearby elliptical galaxies by Thomas et al. (2005), for ellipticals

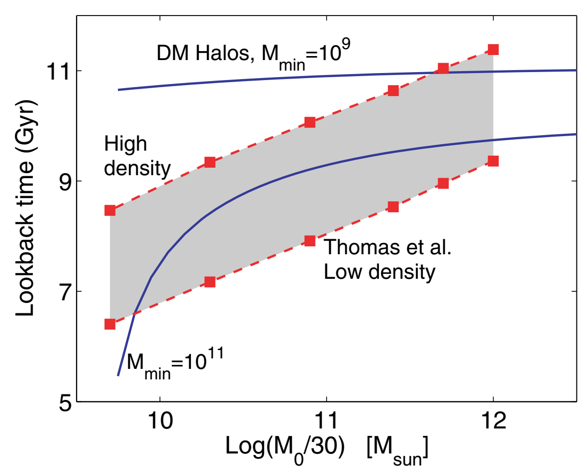

Figure 11. Effective formation epoch versus mass in EPS theory versus observations. The formation epoch for DM haloes of present mass M_0, based on equation (26), is plotted for $M_{\min} = 10^9$ and 10^{11} $\mathrm{M}_{\odot}$ (solid curves). Halo masses are divided by 30 in order to roughly translate DM into stellar masses. The epoch for star formation as deduced from local ellipticals by Thomas et al. (2005) is shown (shaded area) between the two dashed lines which refer to galaxies in low- and high-density environments. Here $h = 0.75$ as in Thomas et al. (2005). There is a downsizing behaviour in both cases.

in both low- and high-density environments.[2] The solid lines correspond to our estimates of equation (26) for $M_{\rm min} = 10^9$ and 10^{11} $\mathrm{M}_\odot$, as indicated. Note that we have divided the DM masses by 30 to obtain a very rough proxy for the stellar mass. A comparison with the data of Thomas et al. is only truly meaningful if (i) all gas in haloes with $M > M_{\rm min}$ is turned into stars instantaneously, and (ii) haloes host only one galaxy whose stellar mass is equal to $M_0/30$. Although neither of these is likely to be correct, the data and 'model' are in qualitative agreement in that the more massive structures have formed earlier, i.e. the model shows ADS. If $M_{\rm min} = 10^9\ h^{-1}\ \mathrm{M}_\odot$, the DS strength is too weak, across the mass range of interest, compared to the data. This indicates that the baryonic physics need to delay and/or suppress star formation relatively more in lower mass haloes. Alternatively, if $M_{\rm min}$ is significantly larger ($\sim 10^{11}\ h^{-1}\ \mathrm{M}_\odot$), the DS strength at fixed halo mass is stronger, and there is less need to delay or suppress star formation in order to globally match the data. However, this requires a yet-unknown physical mechanism that can prevent star formation in all haloes below this mass limit.

Yet another way to view the ADS aspect of halo formation histories is via the mean epoch at which a halo of mass M_0 at time ω_0 has a progenitor of mass M. The number density, d $N(\omega)$, of progenitors with masses in the interval M to $M + \mathrm{d}M$ at time ω is given by equation (7). Using it to weight the averaging of ω, we obtain

$$\omega_{\rm p} \equiv \frac{\int \mathrm{d}N(\omega)\omega\,\mathrm{d}\omega}{\int \mathrm{d}N(\omega)\,\mathrm{d}\omega} = \omega_0 + \sqrt{\frac{2}{\pi}(S - S_0)}. \tag{27}$$

This resembles ω_R in equation (26), meaning that the mean formation epoch for a given $M_{\rm min}$ is equivalent to the mean epoch for progenitors to be of a given mass, $M = M_{\rm min}$. The ADS behaviour is apparent in equation (27) from the fact that $\omega_{\rm p}$ increases with M_0 (via S_0). This implies that progenitors *of a given mass* appear earlier in the merger tree of a more massive present-day halo. This is similar to the result obtained by Mouri & Taniguchi (2006), who also argue that downsizing is a natural prediction of hierarchical formation scenarios.

6 DOWNSIZING IN TIME

As mentioned in Section 1, there is another observed downsizing effect, different from the ADS dealt with so far, which refers to the decrease with time of the characteristic mass of the galaxies with the highest SSFR. We show here that, unlike the ADS, this DST is not in general rooted in the hierarchical clustering of DM haloes. The dark haloes show such an effect only if $M_{\rm min}$ is decreasing with time in a sufficiently steep pace.

The symbols in Fig. 12 show the DST obtained from the data in Brinchmann & Ellis (2000). For a given SSFR, we select from their data the stellar mass and redshift of a galaxy with that SSFR. The solid squares, connected by a dotted curve, plot the stellar mass of objects forming their stars with a SSFR of 1 Gyr^{-1}, corresponding to a doubling time-scale $\tau_c = 1$ Gyr. Note that the characteristic stellar mass of systems forming stars at this rate is lower at lower redshift; this is DST. The other symbols correspond to lower SSFRs of 0.1 Gyr^{-1} (solid dots connected by dashed curve) and 0.05 Gyr^{-1} (stars connected by solid curve). Note that each of these curves reveals DST, and that more massive systems have lower SSFRs, at each redshift.

[2]The density is defined as the number of galaxies within one-degree radius [see Thomas et al. (2005) for details].

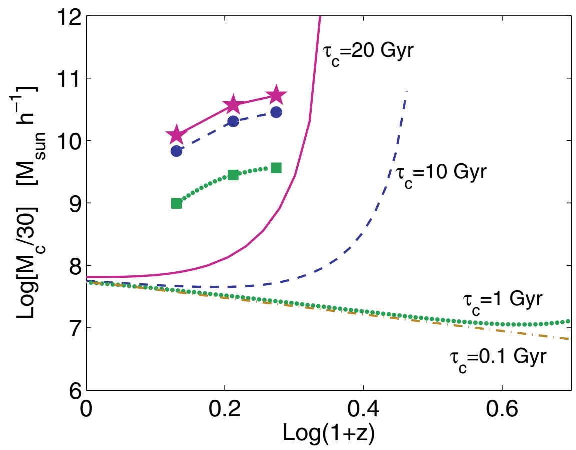

Figure 12. The mass of haloes which form at a given rate R_c at z, $M_c(R = R_c, z)$ from equation (29). The curves are marked by $\tau_c = R_c^{-1}$. For high enough τ_c, the mass M_c depends solely on dω/dt, while for low τ_c it is given by $M_c(z) = M_{\rm min}(z)$. The connecting symbols refer to the observed star formation time-scale for galaxies of a given stellar mass from fig. 3 of Brinchmann & Ellis (2000), for the corresponding values of τ_c. The M_c values for the dark haloes were divided by 30 in order to allow a crude comparison with the stellar mass of the galaxies.

In order to compare this with DM haloes, we define the 'current', specific formation rate of DM haloes as the rate of change of $M_{\rm all}$ normalized to $M_{\rm all}$. This rate is obtained by setting $\omega = \omega_0$ in the general expression for $R(\omega\,|\,\omega_0, M_0)$ of equation (24):

$$R(\omega\,|\,\omega, M_0) = -\sqrt{\frac{2}{\pi}}\frac{1}{\sqrt{S_{\rm min}(z) - S(M_0)}}\frac{\mathrm{d}\omega}{\mathrm{d}t}(z). \tag{28}$$

For a fixed rate $R = R_c$, one can solve for $M_c(z)$, the mass of haloes that are formed with the rate R_c:

$$S\,[M_c(z)] = S_{\rm min}(z) - \frac{2}{\pi}\left(\frac{\mathrm{d}\omega}{\mathrm{d}t}\right)^2 \tau_c^2, \tag{29}$$

where $\tau_c \equiv R_c^{-1}$ is the corresponding time-scale. The curves without symbols in Fig. 12 show the $M_c(z)$ relations thus obtained for four different time-scales τ_c, as indicated. In order to allow for a comparison with the data, we have divided the halo masses by 30, as a rough proxy for stellar mass. The first thing to note is that these 'model predictions' have almost nothing in common with the data. First of all, all $M_c(z)$ seem to converge to the same mass at low z, independent of τ_c. This owes to the fact that $R \to \infty$ if $M_0 \to M_{\rm min}$; the specific formation rate becomes infinite at $M_{\rm min}$. Secondly, for high specific formation rates (low τ_c), the $M_c(z)$ decreases with increasing z, opposite to the DST observed. This simply owes to the fact that low τ_c implies that $M_c(z) \sim M_{\rm min}(z)$, which, according to equation (20), decreases with increasing redshift. When τ_c is sufficiently high ($\gtrsim$10 Gyr), however, the dark haloes show a qualitative DST, in that M_c increases with redshift. This basically owes to the fact that the contribution from the dω/dt term in equation (29) becomes dominant over the term governed by the $M_{\rm min}(z)$ behaviour. We conclude that, in general, the formation histories of DM haloes do not show a DST effect as observed for galaxies. It is clear that DST must be driven by baryonic processes, which must strongly decouple the star formation rates from the halo formation rates. The challenge for the models will be to do so while maintaining a fairly tight coupling at high z, which, as we have shown, is required in order to explain the ADS.

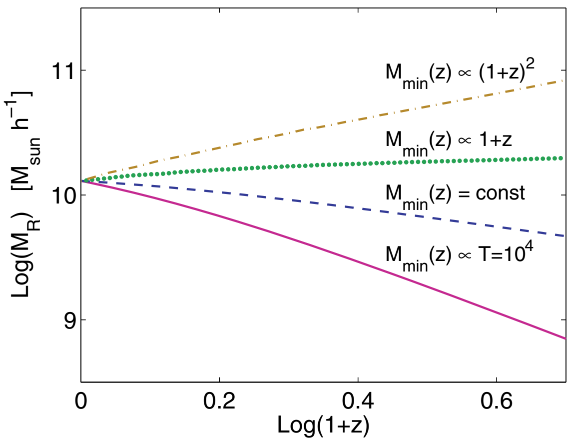

Figure 13. Average halo mass M_R weighted by halo formation rate R as a function of redshift for different z-dependences of $M_{\rm min}(z)$. DST is seen only when $M_{\rm min}(z)$ is increasing linearly with $(1 + z)$ or faster.

Another measure of DST for DM haloes is the time evolution of the average halo mass at which DM is being added to virialized progenitors, namely

$$M_R = \frac{\int R(\omega\,|\,\omega, M) M \frac{\mathrm{d}n}{\mathrm{d}M} \mathrm{d}M}{\int R(\omega\,|\,\omega, M) \frac{\mathrm{d}n}{\mathrm{d}M} \mathrm{d}M}. \tag{30}$$

Here, R is given by equation (28) and $\mathrm{d}n/\mathrm{d}M$ is the number density of haloes per comoving volume (e.g. from Sheth & Tormen 2002).

In Fig. 13, we plot M_R for several different growth rates of $M_{\rm min}(z)$, all normalized to coincide with our standard value of $M_{\rm min}$ at $z = 0$. Similar to M_c defined above, the characteristic mass M_R is decreasing with redshift when we set $M_{\rm min}$ to correspond to a constant virial temperature $T_{\rm vir} = 10^4$ K (see equation 20), or when $M_{\rm min}$ is constant in time. Only when $M_{\rm min}$ is increasing with redshift roughly as $1 + z$ or faster does the mass M_R show a DST behaviour.

7 CONCLUSIONS

We have introduced a new quantity to quantify the growth of a DM halo merger tree, $M_{\rm all}(z)$, the sum of the masses of all the virialized progenitors at redshift z down to a minimum halo mass $M_{\rm min}(z)$. We have shown, using EPS theory, that this quantity reveals an 'ADS' behaviour in that $M_{\rm all}(z)$ of more massive haloes grew earlier and on shorter time-scales. This behaviour is present for any choice of non-zero $M_{\rm min}(z)$ and any cosmology. The only two conditions are (i) that the threshold mass $M_{\rm min}(z)$ is independent of the mass M_0 of the present-day halo, and (ii) that the progenitor mass function, $P(M_1, z_1\,|\,M_0, z_0)$ (equation 6) either depends on $S(M_0) - S(M_1)$ alone (i.e. the trajectories $\delta(S)$ are Markovian) or is such that the fraction of mass in progenitors below $M_{\rm min}$ decreases with increasing M_0. The fact that a similar ADS effect is revealed by EPS merger trees and in N-body simulations indicates that these conditions are, at least, approximately valid. One should note that the first condition, although quite robust, might be violated in certain circumstances. For example, today's halo mass M_0 could be interpreted at high z as reflecting the local environment density, and if the threshold mass is somehow affected by its environment this could introduce a dependence of $M_{\rm min}(z)$ on M_0.

Using the EPS formalism, we have analytically formulated the virial mass growth curve $M_{\rm all}(z)$, the corresponding formation redshift $z_{\rm all}$ and the formation rate. The latter is found to be qualitatively similar to the formation rate of stars in elliptical galaxies, indicating that the observed ADS in these systems has its roots in the formation histories of the DM haloes. However, $M_{\rm all}(z)$ is only a good tracer of the star formation histories of galaxies if all the gas in haloes with $M > M_{\rm min}$ forms stars instantaneously. In reality, this will not be the case, as cooling and various feedback processes can delay and/or prevent the formation of stars, even in haloes with $M \gg M_{\rm min}$. What is clear from our study, however, is that the halo mass dependence of these baryonic processes has to be such that it does not undo the mass dependence already encoded in $M_{\rm all}(z)$.

We have also studied the more common halo assembly histories, defined as the mass growth histories, $M_{\rm main}(z)$, of the main progenitor of the merger tree. We have developed an analytical approximation for it based on EPS theory, and confirmed the known 'upsizing' behaviour of this assembly history. We have shown that it depends, in principle, on the shape of the power spectrum, but it is valid for all power-law spectra as well as for the CDM power spectrum. The formation times $z_{\rm main}$ and $z_{\rm all}$, for a sample of equal-mass haloes, were found to be correlated in a way that can be understood in terms of the mass growth at low redshifts.

The DST, namely the decline with time of the mass of star-forming galaxies, cannot be easily traced back to the properties of the DM halo merger trees. With our idealized recipe of rapid star formation in virialized haloes above $M_{\rm min}(z)$, DST can be reproduced only if $M_{\rm min}(z)$ is rapidly increasing with z. Otherwise, this kind of downsizing is most likely a result of feedback effects on star formation, which requires a more sophisticated modelling of the baryonic processes. The lesson is that the different faces of 'downsizing' reflect different phenomena, one naturally rooted in the hierarchical DM clustering process and the other determined by non-trivial baryonic processes, which are yet to be properly modelled.

ACKNOWLEDGMENTS

We thank Risa Wechsler for providing the merger trees constructed from cosmological N-body simulations based on work supported by NASA ATP NAG5-8218 (Primack and Dekel). We acknowledge stimulating discussions with Itai Arad and Aaron Dutton. This research has been supported by ISF 213/02 and by the German–Israel Einstein Center at HUJI. AD acknowledges support from a Blaise Pascal International Chair in Paris.

REFERENCES

Bardeen J. M., Bond J. R., Kaiser N., Szalay A. S., 1986, ApJ, 304, 15
Baugh C. M., Cole S., Frenk C. S., 1996, MNRAS, 283, 1361
Bell E. F., Baugh C. M., Cole S., Frenk C. S., Lacey C. G., 2003, MNRAS, 343, 367
Bell E. F. et al., 2005, ApJ, 625, 23
Binney J., 2004, MNRAS, 347, 1093
Birnboim Y., Dekel A., 2003, MNRAS, 345, 349
Bond J. R., Cole S., Efstathiou G., Kaiser N., 1991, ApJ, 379, 440
Bower R. G., 1991, MNRAS, 248, 332
Bower R. G., Benson A. J., Malbon R., Helly J. C., Frenk C. S., Baugh C. M., Cole S., Lacey C. G., 2006, MNRAS, 370, 645
Brinchmann J., Ellis R. S., 2000, ApJ, 536, L77
Bryan G. L., Norman M. L., 1998, ApJ, 495, 80
Bundy K. et al., 2005, preprint (astro-ph/0512465)
Cattaneo A., Dekel A., Devriendt J., Guiderdoni B., Blaizot J., 2006, MNRAS, 370, 1651
Cowie L. L., Songaila A., Hu E. M., Cohen J. G., 1996, AJ, 112, 839
Croton D. J. et al., 2006, MNRAS, 365, 11
Dekel A., Birnboim Y., 2006, MNRAS, 368, 2
Dekel A., Silk J., 1986, ApJ, 303, 39

De Lucia G., Springel V., White S. D. M., Croton D., Kauffmann G., 2006, MNRAS, 366, 499
Eisenstein D. J., Loeb A., 1996, ApJ, 459, 432
Firmani C., Avila-Reese V., 2000, MNRAS, 315, 457
Gao L., Springel V., White S. D. M., 2005, MNRAS, 363, L66
Guzman R., Gallego J., Koo D. C., Phillips A. C., Lowenthal J. D., Faber S. M., Illingworth G. D., Vogt N. P., 1997, ApJ, 489, 559
Harker G., Cole S., Helly J., Frenk C., Jenkins A., 2006, MNRAS, 367, 1039
Heavens A., Panter B., Jimenez R., Dunlop J., 2004, Nat, 428, 625
Hernquist L., Springel V., 2003, MNRAS, 341, 1253
Jimenez R., Panter B., Heavens A. F., Verde L., 2005, MNRAS, 356, 495
Juneau S. et al., 2005, ApJ, 619, L135
Kauffmann G., 1996, MNRAS, 281, 487
Kauffmann G., Charlot S., 1998, MNRAS, 294, 705
Kauffmann G., White S. D. M., 1993, MNRAS, 261, 921
Kodama T. et al., 2004, MNRAS, 350, 1005
Lacey C., Cole S., 1993, MNRAS, 262, 627 (LC93)
Lacey C., Cole S., 1994, MNRAS, 271, 676
Li Y., Mo H. J., van den Bosch F. C., 2005, preprint (astro-ph/0510372)
Mouri H., Taniguchi Y., 2006, preprint (astro-ph/0601042)
Nelan J. E., Smith R. J., Hudson M. J., Wegner G. A., Lucey J. R., Moore S. A. W., Quinney S. J., Suntzeff N. B., 2005, ApJ, 632, 137
Nusser A., Sheth R. K., 1999, MNRAS, 303, 685
Press W. H., Schechter P., 1974, ApJ, 187, 425
Scannapieco E., Silk J., Bouwens R., 2005, ApJ, 635, L13
Sheth R. K., Tormen G., 2002, MNRAS, 329, 61
Somerville R. S., Kolatt T. S., 1999, MNRAS, 305, 1 (SK99)
Sugiyama N., 1995, ApJS, 100, 281
Thomas D., 1999, MNRAS, 306, 655
Thomas D., Kauffmann G., 1999, in Hubeny I., Heap S., Cornett R., eds, ASP Conf. Ser. 192, Spectrophotometric Dating of Stars and Galaxies Probing Star Formation Time-scales in Elliptical Galaxies. Astron. Soc. Pac., San Francisco, p. 261
Thomas D., Maraston C., Bender R., de Oliveira C. M., 2005, ApJ, 621, 673
van den Bosch F. C., 2002a, MNRAS, 332, 456
van den Bosch F. C., 2002b, MNRAS, 331, 98 (vdB02)
Wechsler R. H., Bullock J. S., Primack J. R., Kravtsov A. V., Dekel A., 2002, ApJ, 568, 52

APPENDIX A: ANALYTICAL FORMULAE FOR $M_{\rm main}$

We use $\bar{M}_{\rm main}(z)$ to denote the main progenitor mass at redshift z, averaged (at fixed z) over many individual merger trees for the same parent mass M_0. Here, we use the EPS formalism to derive an analytical estimate for $\bar{M}_{\rm main}(z)$.

A1 Basic equation

Let us start with a halo of mass M_0 at time ω_0, and take a small time-step, $\Delta\omega$, back in time. At the time $\omega_0 + \Delta\omega$, we want to compute the average mass of the main progenitor. This requires the full probability distribution, $P(M_{\rm main}\,|\,M_0, \Delta\omega)$, that a halo of mass M_0 at ω_0 has a main progenitor of mass $M_{\rm main}$ at time $\omega_0 + \Delta\omega$. For $M_{\rm main} \geqslant M_0/2$, one has that $P(M_{\rm main}\,|\,M_0, \Delta\omega)$ is equal to the total progenitor distribution d $N/{\rm d}M$ given by equation (7), simply because any progenitor whose mass exceeds $M_0/2$ must be the *main* progenitor. For $M_{\rm main} < M_0/2$, however, the only valid condition is that $P \leqslant {\rm d}N/{\rm d}M$, which is not sufficient to predict $P(M_{\rm main}\,|\,M_0, \Delta\omega)$.

As a first naive approximation, we assume that $P(M_{\rm main}\,|\,M_0, \Delta\omega) = 0$ for $M_{\rm main} < M_0/2$, so that the main progenitor always has a mass $M_{\rm main} \geqslant M_0/2$. Using this approximation, the average mass of the main progenitor, $\bar{M}_{\rm main}(\Delta\omega)$, can be written as

$$\bar{M}_{\rm main}(\Delta\omega) = \int_{M_0/2}^{M_0} P(M\,|\,M_0, \Delta\omega) M\,{\rm d}M. \tag{A1}$$

Using the definition of ${\rm d}N/{\rm d}M$, this reduces to

$$\bar{M}_{\rm main}(\Delta\omega) = M_0\left[1 - {\rm erf}\left(\frac{\Delta\omega}{\sqrt{2S_2 - 2S_0}}\right)\right], \tag{A2}$$

with $S_2 = S(M_0/2)$ and $S_0 = S(M_0)$.

We assume that M_0 is just the main progenitor of the previous time-step.[3] The rate of change, ${\rm d}\bar{M}_{\rm main}/{\rm d}\omega$, can then be computed as

$$\begin{aligned}\frac{{\rm d}\bar{M}_{\rm main}}{{\rm d}\omega} &= \lim_{\Delta\omega\to 0}\frac{\bar{M}_{\rm main}(\Delta\omega) - M_0}{\Delta\omega}\\ &= -M_0\lim_{\Delta\omega\to 0}\frac{1}{\Delta\omega}{\rm erf}\left(\frac{\Delta\omega}{\sqrt{2S_2 - 2S_0}}\right).\end{aligned} \tag{A3}$$

Using the limit ${\rm erf}(x) \to 2x/\sqrt{\pi}$ when $x \to 0$ yields

$$\frac{{\rm d}\bar{M}_{\rm main}}{{\rm d}\omega} = -\sqrt{\frac{2}{\pi}}\frac{\bar{M}_{\rm main}}{\sqrt{S_2 - S}}. \tag{A4}$$

In the case of scale-free initial conditions, where the power spectrum is a pure power law ($S \propto M^{-\alpha}$), we can solve for $\bar{M}_{\rm main}$ analytically:

$$\bar{M}_{\rm main}(\omega) = \left[M_0^{-\frac{\alpha}{2}} + c_\alpha(\omega - \omega_0)\right]^{-\frac{2}{\alpha}}, \tag{A5}$$

where $c_\alpha = \alpha\;[2\pi S(M=1)\,(2^\alpha - 1)]^{-1/2}$.

The above derivation is based on the assumption that the main progenitor always has a mass $M_{\rm main} \geqslant M_0/2$ in the limit $\Delta\omega \to 0$. However, as we show below, when $\Delta\omega \to 0$ the probability that $M_{\rm main} < M_0/2$ decrease like $\Delta\omega$. Consequently, this will give a non-negligible effect for sufficiently large ω.

A2 Towards better accuracy

The dot–dashed line in Fig. A1 shows the distribution of the main progenitor masses of a halo of mass $M_0 = 10^{12}\,h^{-1}\,{\rm M}_\odot$ in a single time-step $\Delta\omega = 0.1$, obtained from 10 000 realizations based on the SK99 algorithm. One can clearly see that $P(M_{\rm main}\,|\,M_0, \Delta\omega)$ has a non-negligible tail for $M_{\rm main} < M_0/2$. The following analysis aims to find the solution for $\bar{M}_{\rm main}$ taking this low-mass tail into account.

The correct shape of $P(M_{\rm main}\,|\,M_0, \Delta\omega)$ can be constrained by the following conditions.

(i) The integral of $P(M_{\rm main}\,|\,M_0, \Delta\omega)$ over all masses should equal unity, for all time-steps $\Delta\omega$.

(ii) $P(M_{\rm main}\,|\,M_0, \Delta\omega) = {\rm d}N/{\rm d}M$, for $M_{\rm main} \geqslant M_0/2$ (equation 7), and $P(M_{\rm main}\,|\,M_0, \Delta\omega) \leqslant {\rm d}N/{\rm d}M$, for $M_{\rm main} < M_0/2$.

(iii) $P(M_{\rm main}\,|\,M_0, \Delta\omega)$ should not depend on the time-step subdivisions. This can be written as

$$\begin{aligned}&P(M_{\rm main}\,|\,M_0, \Delta\omega_1 + \Delta\omega_2)\\ &\quad= \int P(M_1|M_0, \Delta\omega_1)P(M_{\rm main}|M_1, \Delta\omega_2){\rm d}M_1.\end{aligned} \tag{A6}$$

[3]Equation (A2) becomes linear in $\Delta\omega$ for small enough $\Delta\omega$, and this gives $\bar{M}_{\rm main}(\Delta\omega_1 + \Delta\omega_2|M_0) = \bar{M}_{\rm main}[\Delta\omega_2|\bar{M}_{\rm main}(\Delta\omega_1|M_0)]$.

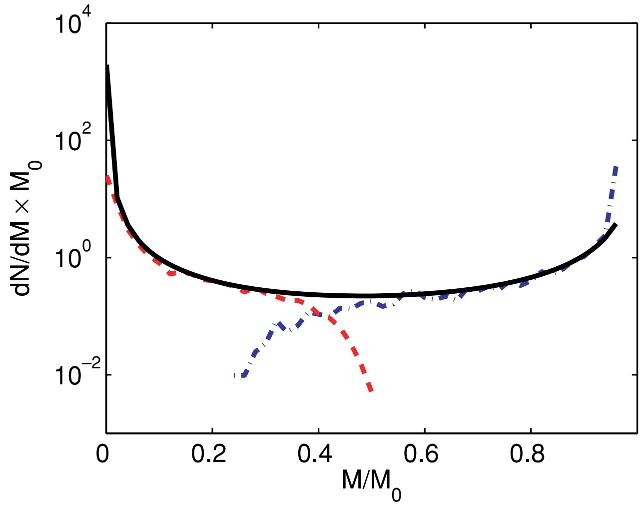

Figure A1. Average number of progenitors of mass M one time-step $\Delta\omega = 0.1$ before the present for halo of mass $M_0 = 10^{12}\,h^{-1}\,\mathrm{M}_{\odot}$. The solid curve is the theoretical prediction. The dot–dashed lines indicate that mass distribution of the main progenitor (defined as the most massive progenitor), as obtained from 10 000 Monte Carlo EPS realizations based on the SK99 algorithm. Note that the probability distribution for the mass of the main progenitor equals d N/dM down to $M_0/2$, but does not vanish down to $M \sim 0.25M_0$. Finally, the dashed line indicates the mass distribution of the least-massive progenitors obtained in these 10 000 realizations.

In what follows, we estimate the limits on $P(M_{\rm main} \mid M_0, \Delta\omega)$ using conditions (i) and (ii), and show that they give a narrow range for $\bar{M}_{\rm main}(z)$. Condition (iii) does not force the solution to be unique, hence it enables a set of solutions, each of them is valid within the EPS formalism. Because condition (iii) is more difficult to implement, we do not compute its effect on $\bar{M}_{\rm main}$, and assume that it will not significantly affect the range of solutions.

The first condition on $P(M_{\rm main} \mid M_0, \Delta\omega)$ is that its integral equals unity. We define $n_{\rm tail}$ as the integral over $P(M_{\rm main} \mid M_0, \Delta\omega)$ from $M_{\rm main} = 0$ to $M_{\rm main} = M_0/2$:

$$n_{\rm tail} = 1 - \frac{M_0}{\sqrt{2\pi}} \int_{S_0}^{S_2} \frac{1}{M} \frac{\Delta\omega}{\Delta S^{1.5}} \exp\left(-\frac{\Delta\omega^2}{2\Delta S}\right) \mathrm{d}S, \tag{A7}$$

where $\Delta S = S - S_0 = S(M) - S(M_0)$.

We can estimate the possible effect *any* tail will have on $\bar{M}_{\rm main}$ by computing the effect of the most extreme tails possible. The first extreme is to concentrate all the tail in a small range near $M = 0$. In this case, the integral of $M_{\rm main}\, P(M_{\rm main} \mid M_0, \Delta\omega)$ over the range $0 \leqslant M_{\rm main} < M_0/2$ will be zero. As a result, the $\bar{M}_{\rm main}(z)$ that corresponds to this extreme is given by equation (A2). The second extreme is that all the tail is concentrated near $M_0/2$, that is, $P(M_{\rm main} \mid M_0, \Delta\omega)$ has its maximum values ($=$ dN/dM) down to a lower mass limit, $M/q_{\rm max}$, which is set by the requirement that

$$n_{\rm tail} = \frac{M_0}{\sqrt{2\pi}} \int_{S_2}^{S_{q+}} \frac{1}{M} \frac{\Delta\omega}{\Delta S^{1.5}} \exp\left(-\frac{\Delta\omega^2}{2\Delta S}\right) \mathrm{d}S, \tag{A8}$$

where $S_{q+} = S(M/q_{\rm max})$. If we focus our attention on small time-steps $\Delta\omega$, then we can use that d $P(M_{\rm main} \mid M_0, \Delta\omega)/\mathrm{d}M_{\rm main} \simeq 0$ near $M_0/2$ to approximately write that

$$S_{q+} \simeq S_2 + \sqrt{\frac{\pi}{2}} \frac{(S_2 - S_0)^{1.5}}{\Delta\omega} n_{\rm tail}. \tag{A9}$$

This enables us to use a simple equation for S_{q+}, combined with the definition of $n_{\rm tail}$ in equation (A7).

What remains is to find an appropriate expression for $n_{\rm tail}$ which is valid in the limit of small time-steps $\Delta\omega$. We therefore split the integral in equation (A7) into two parts. The first one (n_1) is for the range $0 < \Delta S < \Delta S_\epsilon$, where $\Delta\omega \ll \Delta S_\epsilon \ll 1$ and we can make the approximation $M \sim M_0$:

$$n_1 \simeq \frac{1}{\sqrt{2\pi}} \int_{S_0}^{S_0+\Delta S_\epsilon} \frac{\Delta\omega}{\Delta S^{1.5}} \exp\left(\frac{-\Delta\omega^2}{2\Delta S}\right) \mathrm{d}S$$

$$= 1 - \mathrm{erf}\left[\frac{\Delta\omega}{\sqrt{2\Delta S_\epsilon}}\right] \simeq 1 - \sqrt{\frac{2}{\pi}} \frac{\Delta\omega}{\sqrt{\Delta S_\epsilon}}. \tag{A10}$$

The second range (n_2) is for $\Delta S > \Delta S_\epsilon$ where the approximation $\exp[-\Delta\omega^2/(2\Delta S)] \simeq 1$ is valid:

$$n_2 \simeq \frac{M_0}{\sqrt{2\pi}} \int_{S_0+\Delta S_\epsilon}^{S_2} \frac{1}{M} \frac{\Delta\omega}{\Delta S^{1.5}} \mathrm{d}S. \tag{A11}$$

Combining equations (A7), (A10) and (A11) then yields

$$n_{\rm tail} = \sqrt{\frac{2}{\pi}} \Delta\omega \left(\Delta S_\epsilon^{-0.5} - \frac{M_0}{2} \int_{S_0+\Delta S_\epsilon}^{S_2} \frac{1}{M} \frac{\mathrm{d}S}{\Delta S^{1.5}} \right). \tag{A12}$$

Finally, we take the limit $\Delta S_\epsilon \rightarrow 0$, and obtain

$$n_{\rm tail} = \sqrt{\frac{2}{\pi}} \Delta\omega \left(\frac{1}{2} \int_0^{S_2-S_0} \frac{M - M_0}{M} \frac{\mathrm{d}\Delta S}{\Delta S^{1.5}} + \frac{1}{\sqrt{S_2 - S_0}} \right). \tag{A13}$$

Substitution in (A9) then yields

$$S_{q+} \simeq 2S_2 - S_0 + \frac{(S_2 - S_0)^{1.5}}{2} \int_0^{S_2-S_0} \frac{M - M_0}{M} \frac{\mathrm{d}\Delta S}{\Delta S^{1.5}}, \tag{A14}$$

independent of $\Delta\omega$. For the standard ΛCDM cosmology, this yields $2.1 < q_{\rm max} < 2.3$ for $0.1 < \Omega_{\rm m} \leqslant 0.9$ and $10^8\,h^{-1}\,\mathrm{M}_{\odot} \leqslant M_0 \leqslant 10^{15}\,h^{-1}\,\mathrm{M}_{\odot}$. This implies that although there is a negligible probability that the main progenitor has a mass $M_0/2.3 < M_{\rm main} < M_0/2$ when $\Delta\omega \rightarrow 0$, this probability behaves like $\Delta\omega$ and it cannot be neglected. We can take this into account by rewriting equation (A4) as

$$\frac{\mathrm{d}\bar{M}_{\rm main}}{\mathrm{d}\omega} = -\sqrt{\frac{2}{\pi}} \frac{\bar{M}_{\rm main}}{\sqrt{S_q - S}}, \tag{A15}$$

with $S_q = S(M_0/q)$ and $2 \leqslant q \lesssim 2.3$. In principle, any value of q in the range above is allowed. In particular, merger trees constructed using different algorithms may have different values of q in the above range, as long as the algorithms adopt a sufficiently small time-step $\Delta\omega$.

In Fig. A2, we show $\bar{M}_{\rm main}$ for a halo of mass $5 \times 10^{12}\,h^{-1}\,\mathrm{M}_{\odot}$. The triangles show the results obtained from many independent EPS merger trees, constructed using the SK99 algorithm. Note that the averaging is done over $M_{\rm main}(z)$ at fixed z, which is the same as done in the analytical estimates (equation A1). The dashed, solid and dotted lines correspond to the analytical prediction of equation (A15) for $q = 2$, 2.2 and 2.5, respectively. The curve for $q = 2.2$ is in excellent agreement with the EPS merger trees. Note that this value for q is within the expected range. In Fig. 3, we show that our analytical formula with $q = 2.2$ also accurately fits the merger-tree results for other values of M_0.

A3 A universal fitting function

Equation (A15) can be solved to obtain a direct, analytical formula for $\bar{M}_{\rm main}(z)$. We use the fitting function for $S(M)$ given in vdB02:

$$S(M) = g^2 \left(\frac{c\Gamma}{\Omega_{\rm m}^{1/3}} M^{1/3} \right) \frac{\sigma_8^2}{g^2(32\Gamma)}, \tag{A16}$$

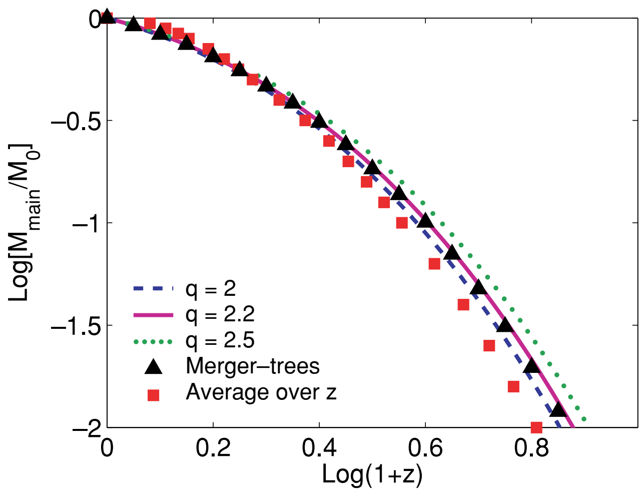

Figure A2. The mass of the main progenitor as computed in different ways for $M_0 = 5 \times 10^{12}\,h^{-1}\,\mathrm{M}_\odot$. Big circles are from vdB02. Squares are the average of EPS merger trees, averaged over z at a fixed M. Triangles are from the same merger trees but averaged over M at a fixed z. Dashed lines show the theoretical limits of the analytic formula ($q = 2$ and 2.5). The solid line is the analytic formula with $q = 2.2$.

where $c = 3.804 \times 10^{-4}$, and $g(x)$ is an analytical function:

$$g(x) = 64.087(1 + 1.074x^{0.3} - 1.581x^{0.4} + 0.954x^{0.5} - 0.185x^{0.6})^{-10}. \tag{A17}$$

In terms of the new set of variables

$$\widehat{M} = M\frac{\Gamma^3}{\Omega_\mathrm{m}},\ \widehat{\omega} = \omega\frac{g(32\Gamma)}{\sigma_8},\ \widehat{g}(x) = g(cx^{1/3}), \tag{A18}$$

equation (A15) does not depend on cosmology, and can be easily solved to give

$$\widehat{M} = F_q^{-1}[\widehat{\omega} - \widehat{\omega}_0 + F_q(\widehat{M}_0)], \tag{A19}$$

where

$$F_q(\widehat{M}) = -\sqrt{\frac{\pi}{2}}\int_0^{\widehat{M}} \frac{\sqrt{\widehat{g}^2(\widehat{M'}/q) - \widehat{g}^2(\widehat{M'})}}{\widehat{M'}}\mathrm{d}\widehat{M'}. \tag{A20}$$

Finally, we write the solution in the original variables:

$$\bar{M}_\mathrm{main}(\omega) = \frac{\Omega_\mathrm{m}}{\Gamma^3}F_q^{-1}\left[\frac{g(32\Gamma)}{\sigma_8}(\omega - \omega_0) + F_q\left(\frac{\Gamma^3}{\Omega_\mathrm{m}}M_0\right)\right]. \tag{A21}$$

The analytical fitting function for $F_q(u)$ with $q = 2.2$ is

$$\begin{aligned} F_q(u) = {} & -6.92 \times 10^{-5}\ln^4 u + 5.0 \times 10^{-3}\ln^3 u \\ & + 8.64 \times 10^{-2}\ln^2 u - 12.66\ln u + 110.8, \end{aligned} \tag{A22}$$

which is accurate to better than 1 per cent over the range $1.6 \times 10^4 < M\Gamma^3\Omega_\mathrm{m}^{-1} < 1.6 \times 10^{13}\,h^{-1}\,\mathrm{M}_\odot$.

A4 An alternative method

We now present an alternative method to compute $M_\mathrm{main}(z)$, which is based on the method originally introduced by LC93. The LC93 argument is as follows. At a specific redshift z, one can compute the probability for having a progenitor with a mass larger than $M_0/2$. This probability equals the probability that a tree will have its z_main greater than z [where z_main is defined by $M_\mathrm{main}(z_\mathrm{main}) = M_0/2$]. Although LC93 claim their formula is only an approximation, we have not found any gap in their argument, so we think this should be an accurate prediction.

Let us define $Q(\omega_1 \mid M_0, \omega_0)$ as the probability that a halo with mass M_0 at time ω_0 will have its merger tree obey $\omega(z_\mathrm{main}) = \omega_1$. The probability for having a progenitor with mass bigger than $M_0/2$ then equals

$$\int_{S_0}^{S_2}\frac{M_0}{M}f(S - S_0, \omega - \omega_0)\,\mathrm{d}S = \int_{\omega}^{\infty} Q(\omega_1 \mid M_0, \omega_0)\,\mathrm{d}\omega_1, \tag{A23}$$

where f is as defined in equation (5), $S_0 = S(M_0)$ and $S_2 = S(M_0/2)$. The distribution $Q(\omega \mid M_0, \omega_0)$ is obtained by differentiating the above equation with respect to ω and multiplying it by -1. In order to compute the mean formation time, we need to average ω over the probability distribution Q:

$$\begin{aligned} \bar{\omega}_{\mathrm{main},1} = {} & \int_{\omega_0}^{\infty}\omega Q(\omega \mid M_0, \omega_0)\,\mathrm{d}\omega = \\ & -\int_{\omega_0}^{\infty}\omega\mathrm{d}\omega\frac{\partial}{\partial\omega}\int_0^{S_2 - S_0}\frac{M_0}{M(S_0 + \Delta S)}f(\Delta S, \Delta\omega)\mathrm{d}\Delta S. \end{aligned} \tag{A24}$$

Here, $\bar{\omega}_{\mathrm{main},1}$ is obtained by averaging over all ω (time) possible for getting a mass $M_0/2$. This is different from the method used above, where ω_main was computed by averaging the main progenitor masses at a fixed time. The two methods should give slightly different results, even if both are accurate. This is illustrated in Fig. A2 where the triangles indicate the average, main progenitor history obtained by averaging over M_main at fixed z, while the squares show the results obtained when averaging over z at fixed M_main.

So far, we have repeated the analysis in LC93. Now, instead of computing the derivative of equation (A23), we simplify equation (A24) by a simple integration by parts:

$$\begin{aligned} \bar{\omega}_{\mathrm{main},1} = {} & -\omega\left[\int_0^{S_2 - S_0}\frac{M_0}{M}f(\Delta S, \Delta\omega)\mathrm{d}\Delta S\right]_{\omega_0}^{\infty} \\ & + \int_{\omega_0}^{\infty}\mathrm{d}\omega\int_0^{S_2 - S_0}\frac{M_0}{M(S_0 + \Delta S)}f(\Delta S, \Delta\omega)\mathrm{d}\Delta S. \end{aligned} \tag{A25}$$

The left-hand part is just ω_0.[4] We can switch the integrals on the right-hand side of the equation, and compute the integral over ω first. Finally, we have

$$\bar{\omega}_{\mathrm{main},1} - \omega_0 = \frac{M_0}{\sqrt{2\pi}}\int_0^{S_2 - S_0}\frac{\mathrm{d}\Delta S}{M(S_0 + \Delta S)\sqrt{\Delta S}}. \tag{A26}$$

For a self-similar power spectrum with $S \propto M^{-\alpha}$, the integral can be done analytically:

$$\bar{\omega}_{\mathrm{main},1} - \omega_0 = \sqrt{\frac{2}{\pi}(S_2 - S_0)}\,{}_2F_1\left(\frac{1}{2}, -\frac{1}{\alpha}, \frac{3}{2}, 1 - 2^{\alpha}\right), \tag{A27}$$

where ${}_2F_1$ is the Gauss hypergeometric function. We can see that $(\bar{\omega}_{\mathrm{main},1} - \omega_0)/\sqrt{S_2 - S_0}$ has the same value for all masses, and thus it is the natural variable to choose (as was done in LC93). On the other hand, we showed in equation (16) that $(\bar{\omega}_\mathrm{main} - \omega_0)/(\sqrt{S_2} - \sqrt{S_0})$ is also a constant, when the averaging of the trees is made along the mass axis.

The above analysis is still valid, if we replace S_2 with $S(\bar{M}_{\mathrm{main},1})$, so that we can easily generalize this result to obtain $\bar{M}_{\mathrm{main},1}$ in the

[4] One should take care when assigning the integral lower limit. The integral over ΔS should first be computed, similar to the analysis done for equation (A7).

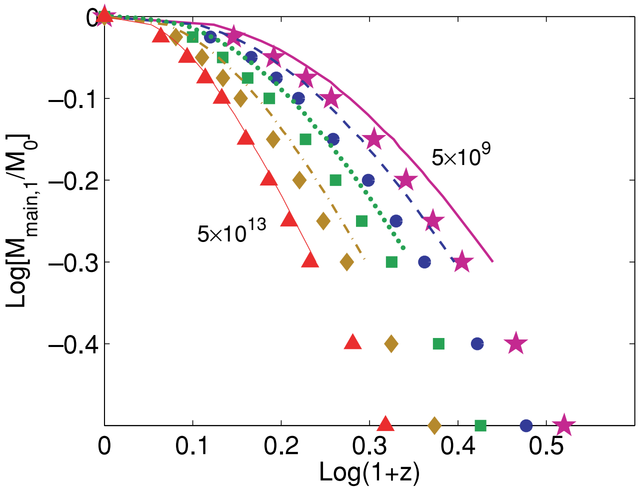

Figure A3. $\bar{M}_{\mathrm{main},1}(z)$ for several halo masses. Symbols are from the merger trees of vdB02. The halo masses range from 5×10^9 to $5 \times 10^{13}\ h^{-1}\ \mathrm{M}_{\odot}$, spaced by a decade. Smoothed lines are the results of the analytic formula, equation (A26), replacing S_2 with $S(\bar{M}_{\mathrm{main},1})$. The equation is valid only for $\bar{M}_{\mathrm{main},1} > M_0/2$.

range $\bar{M}_{\mathrm{main},1} > M_0/2$. For masses below $M_0/2$, however, we cannot compute $\bar{M}_{\mathrm{main},1}$ since this requires the probability for getting a main progenitor with mass lower than $M_0/2$. As discussed above, this part of the probability function is unknown.

In Fig. A3, we compare results from EPS merger-tree realization (vdB02, plotted as symbols) to the analytical formula (smoothed lines). There are some deviations between the two, presumably because the averaging is done over a large range in redshift, where the SK99 algorithm may have slight inaccuracies. This effect can be seen in Fig. 6 and in vdB02 (Fig. 4): the distribution of formation times is only accurate for low values of ω_{main}. Our previous method for computing $\bar{\omega}_{\mathrm{main}}$ was not affected by this inaccuracy because it was derived using the limit of small time-steps behaviour. This, combined with the fact that this method can only be used to compute $\bar{M}_{\mathrm{main}}(z)$ down to $M_0/2$, and the fact that equation (A26) cannot be generalized easily since S_0 is buried inside the integrand, clearly favours the method discussed at the beginning of this appendix over the one discussed here.

This paper has been typeset from a TEX/LATEX file prepared by the author.